UNIVERSITÀ DEGLI STUDI DI PADOVA

Dipartimento di Fisica e Astronomia "Galileo Galilei"

Corso di Laurea in Fisica

Tesi di Laurea

Conceptual design of an energy recovery system from residual ions in the DEMO neutral beam injector

Relatore

Prof. Gianluigi Serianni

Correlatore

Dr. Piero Agostinetti

Laureanda

Alessia D'Anna

Anno Accademico 2017/2018

Contents

Abstract

In order to increase the efficiency of DEMO in this thesis a *conceptual study of purely electrostatic recovery system for negative-ion-besed neutral beam injectors* developed by Jérome Pamela and Stéphane Laffite in 1990-1992 has been resumed and upgraded. Using this project as a starting point, a recovery system substitute for RID(Residual Ion Dump) has been devised, that is an injector component designed for DEMO for the sole absorption of ions without the possibility of collection.
The apparatus in question will be able to collect the residual ions in order to charge an energy storage system and therefore increase the efficiency of the experiment. The collection system foresees that the ions are deflected with respect to the neutral beam, in order to be directed on the collectors and then collected by electrodes. For the deflection of ions, both electric and magnetic methods were considered and, for the latter, a study was carried out on the geometry of the coils in order to optimize the magnetic field in the affected area. The electrical potentials and currents used for the various configurations have been optimized through simulation of the trajectories of positive and negative ions using COMSOL Multiphysics, paying particular attention to the physical limits of thermal load for the vendors and to the RAMI(reliability, availability, maintainability and inspectability) guidelines. To verify the correctness of the results obtained the simulations were validated against analytical computations in simplified cases. Finally, a comparison was made between the various configurations to identify the best solution among them.

Sommario

Al fine di aumentare l'efficienza di DEMO, in questa tesi è stato ripreso e migliorato uno *studio concettuale del sistema di recupero puramente elettrostatico per iniettori di fasci neutri a ioni negativi* sviluppato da Jérome Pamela e Stéphane Laffite nel (1990-1992). Utilizzando questo progetto come punto di partenza, è stato ideato un sistema di recupero sostitutivo al RID(Residual Ion Dump), ovvero un componente dell'iniettore progettato per DEMO finalizzato al solo assorbimento degli ioni senza possibilità di raccolta.
L'apparato in questione sarà in grado di raccogliere gli ioni residui al fine di caricare una batteria e quindi aumentare l'efficienza dell'esperimento. Il sistema di raccolta prevede che gli ioni siano deflessi rispetto al fascio di neutri, in modo da essere indirizzati sui dei collettori e quindi raccolti tramite elettrodi. Per la deflessione degli ioni sono stati considerati sia metodi elettrici che magnetici e, per questi ultimi è stato effettuato uno studio sulla geometria delle bobine al fine di ottimizzare il campo magnetico nella zona interessata. I potenziali elettrici e le correnti utilizzate per le varie configurazioni sono state ottimizzate attraverso la simulazione delle traiettorie di ioni positivi e negativi utilizzando COMSOL Multiphysics, prestando particolare attenzione ai limiti fisici di carico termico per i materiali e alle linee guida del RAMI(reliability, availability, maintainability and inspectability). Per verificare la correttezza dei risultati ottenuti le simulazioni sono state validate con calcoli analitici in casi semplificati. Si è infine effettuato un confronto tra le varie configurazioni per individuare la migliore soluzione tra di esse.

Introduction

.

1.1 Nuclear energy

The energy problem is actually one of the most discussed in the world, energy needs increase more slowly than in the past, but from now until 2040 the demand grows further by 30% .The energy sources used from 1970 to 2017, and the forecasts made up to 2040 are shown in figure (1.1) [1].

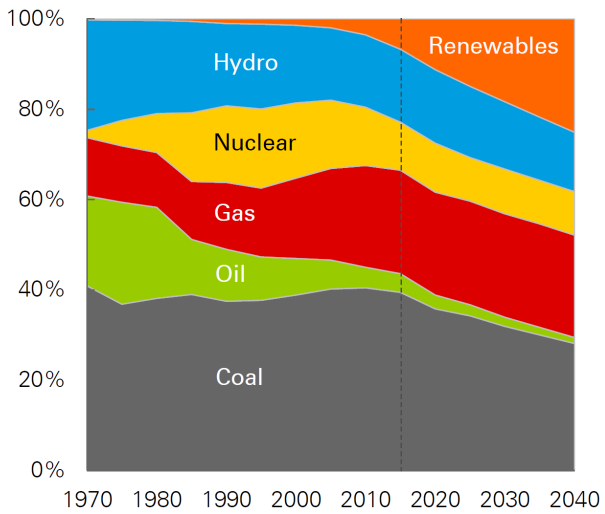

Figure 1.1: Energy sources in use (2017).

Nuclear energy is currently produced by fission, that is by splitting a heavy nucleus (uranium-235 or plutonium-239) with consequent release of energy, however, this procedure has some problems, the important thing is the production of radioactive waste that, together with that of safety, makes this energy solution not much accepted by the world population.
Nuclear fusion is the alternative to which scientific community is working, this occurs between light nuclei having different masses increasing the binding energy and therefore the stability of product. In this a reaction nuclei are approached and consequent occurs electromagnetic repulsion, they join together forming an atom with a minor mass of the sum of masses of reagents and also one or more free neutrons.

[1] BP Statistical Review of World Energy, June 2018

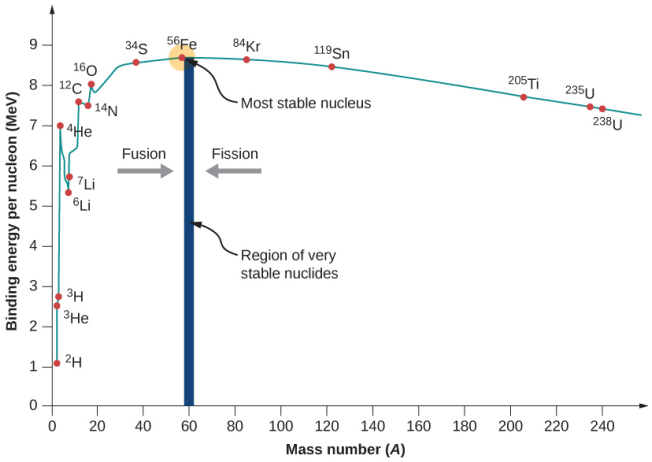

Figure 1.2: Binding energy of nuclei.

Fusion is an esoenergetic process, therefore it releases energy that was previously conserved in the nuclear bond in the form of thermal energy. The amount of heat produced in this process has both advantages and disadvantages, in fact it can be exploited for the production of electricity and energy is comparable or even superior to that produced by fission (around 1 MeV for nucleus), in addition the light nuclei are more abundant in nature and the products are light, stable and non-radioactive, but the temperatures and pressures necessary to support it are very high, because, to melt, a quantity of energy is needed to overcome the Coulomb barrier and it is difficult to control. The kinetic energies of the plasma particles follow the statistical distribution of Maxwell-Boltzmann, therefore the temperatures corresponding to about 1-10 keV are of the order of $10^7 - 10^8$ K. Fusion is also the reaction which is responsible for the energy of sun and stars, in this case gravity controls energy.
Obtaining this reaction in nuclear reactors presents many problems, in fact nuclei deprived of electrons repel themselves and the gas expands ruining the walls of containers, for this reason the magnetic confinement that must be able to contain the plasma is used, but must also allow a fraction of its energy to be transmitted to a calorimeter in order to extract useful energy, it is also necessary to minimize the initial effort and manage the presence of neutrons released by the reaction.
Most interesting reactions are therefore those that do not free neutrons or that do it at low energies:

- D-T reaction (the lower threshold, 50 keV)
  D + T $\rightarrow$ ^{4}He (3.5 MeV) + n (14.1 MeV)
- D-D reaction (this reactions have the same probability to happen)
  D + D $\rightarrow$ T (1.01 MeV) + p (3.02 MeV)
  D + D $\rightarrow$ ^{3}He (0.82MeV) + n (2.45 MeV)
- T-T reaction
  T - T $\rightarrow$ ^{4}He + 2 n (11.3 MeV)

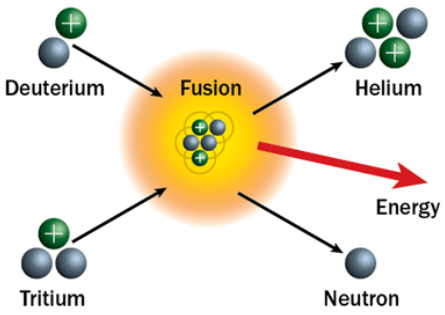

Figure 1.3: Fusion.

1.2 ITER

ITER(International Thermonuclear Experimental Reactor) is an experiment of nuclear fusion currently active that has the goal of achieving a nuclear fusion reactor able to produce more energy than necessary for triggering the reaction. It is a Tokamak that is a toroidal shape machine designed by Russian physicists who, through the magnetic confinement of hydrogen isotopes in the plasma state, creates the conditions for internal thermonuclear fusion to occur in order to extract the energy produced. Another goal that is not less important is the development of new technologies in anticipation of the DEMO realization (of which we will speak in the next paragraph), particularly in the field of cryogenics, superconductivity and high vacuum techniques.
The realization is underway in Cadarache, in the South of France, in collaboration with Europe, Russia, China, Japan, the United States of America, India and South Korea.

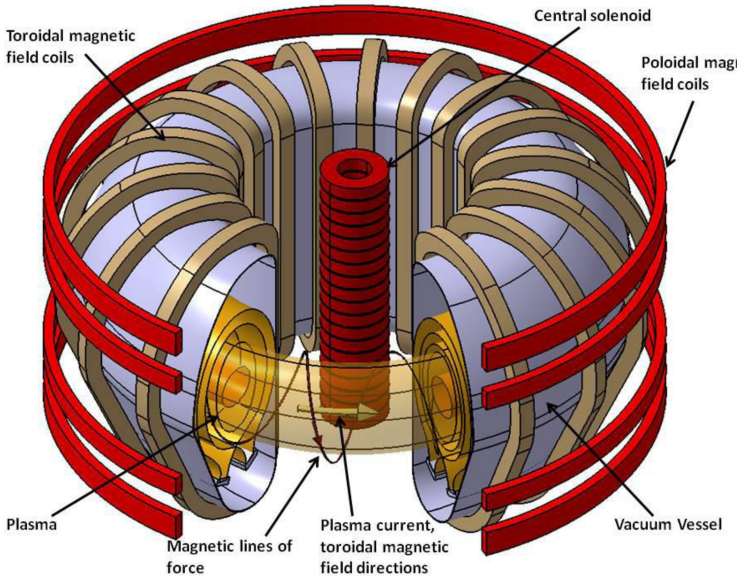

Figure 1.4: ITER magnetic field lines configuration.

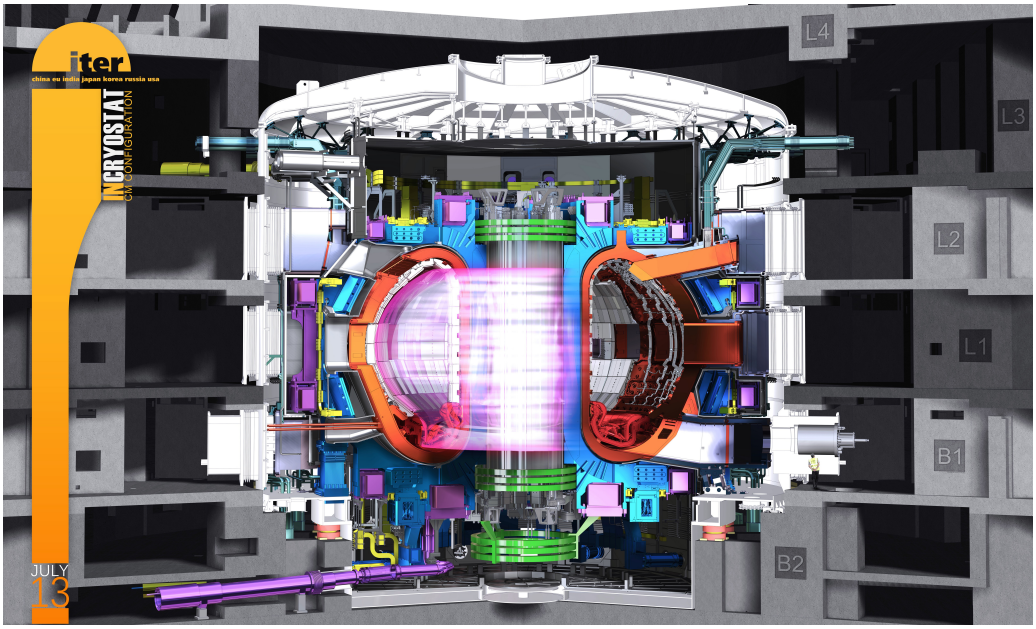

Figure 1.5: ITER experimental reactor cutaway with plasma current.

The power of a Tokamak is capable of producing is a direct result of the number of fusion reactions taking place in its core so, increasing the vessel size also increases the plasma volume and consequently the fusion energy. ITER provides a plasma ten times greater plasma than the largest existing machine and will be a unique experimental tool, capable of longer plasmas and better confinement.
The machine has been designed specifically to [1]:

- **Produce 500 MW of fusion power**
  The world record for fusion power is held by the European Tokamak JET. In 1997, JET produced 16 MW of fusion power from a total input heating power of 24 MW (Q=0.67). ITER is designed to produce a ten-fold return on energy (Q=10), or 500 MW of fusion power from 50 MW of input heating power. ITER will not capture the energy it produces as electricity, but—as first of all fusion experiments in history to produce net energy gain—it will prepare the way for the machine that can.
- **Demonstrate the integrated operation of technologies for a fusion power plant**
  ITER will bridge the gap between today's smaller-scale experimental fusion devices and the demonstration fusion power plants of the future. Scientists will be able to study plasmas under conditions similar to those expected in a future power plant and test technologies such as heating, control, diagnostics, cryogenics and remote maintenance.
- **Achieve a deuterium-tritium plasma in which the reaction is sustained through internal heating**
  Fusion research today is at the threshold of exploring a "burning plasma"—one in which the heat from the fusion reaction is confined within the plasma efficiently enough for the reaction to be sustained for a long duration. Scientists are confident that the plasmas in ITER will not only produce much more fusion energy, but will remain stable for longer periods of time.
- **Test tritium breeding**
  One of the missions for the later stages of ITER operation is to demonstrate the feasibility of producing tritium within the vacuum vessel. The world supply of tritium (used with deuterium to fuel the fusion reaction) is not sufficient to cover the needs of future power plants. ITER will provide a unique opportunity to test mockup in-vessel tritium breeding blankets in a real fusion environment.
- **Demonstrate the safety characteristics of a fusion device**
  ITER achieved an important landmark in fusion history when, in 2012, the ITER Organization was licensed as a nuclear operator in France based on the rigorous and impartial examination of its safety files. One of the primary goals of ITER operation is to demonstrate the control of the plasma and the fusion reactions with negligible consequences to the environment.

1.3 DEMO

The following step after ITER experimental reactor is DEMO(DEMOnstration Fusion Power Plant). This experiment proposes to demonstrate the possibility to produce electric energy from the fusion reaction and to prove the industrial feasibility of this (achievement of a power output in the Q-value range of 30 to 50 (as opposed to ITER's 10)), the safety aspects and the tritium self sufficiency. In order to reduce the costs of electricity produced by this power plant in designing the guidelines are reliability, availability, maintainability and inspectability (RAMI) and efficiency. For this reasons have been introduced several innovative solutions and improvements particularly for the beam source, neutraliser and vacuum pumping systems compared to the ITER NBI(Neutral Beam Injector). In Europe a large R&D effort is devoted to maximizing the efficiency and obtaining the most effective system, respecting the RAMI analysis and the requirements for the DEMO power plant.

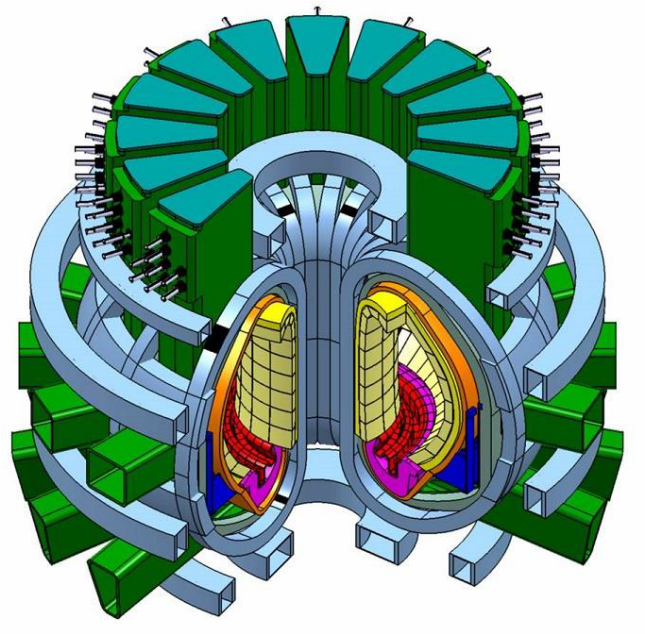

Figure 1.6: DEMO reactor cutaway.

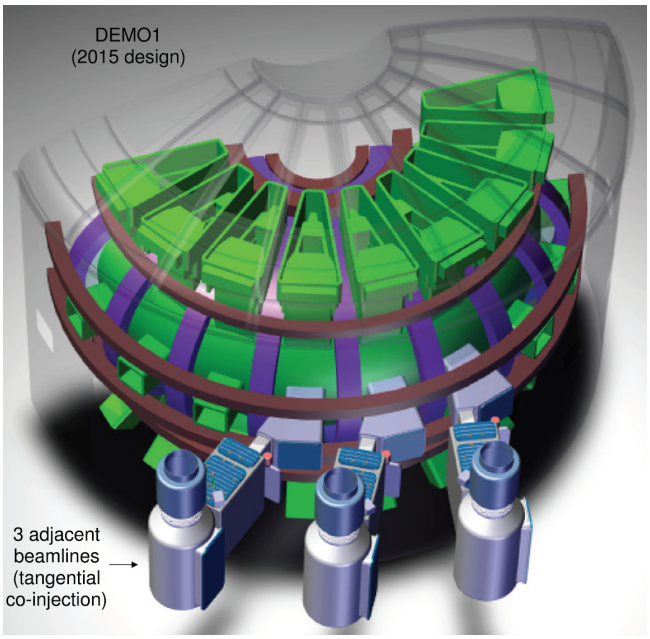

Figure 1.7: Integration of the Heating Neutral Beams in the DEMO1 pre-conceptual design.

Now let's compare the differences of the NBI of ITER and DEMO which is the component that this thesis proposes to optimize (that of DEMO will be discussed in detail below). It can be noted that the requirements of the advanced DEMO NBI are similar but non identical to the ones of the ITER NBI. Namely it can be observed that [2]:

- In DEMO NBI only deuterium negative ions are considered, whereas ITER NBI is also required to operate with hydrogen negative ions. D^0 is the final goal in both NBIs but in ITER experiments with H^0 are foreseen to test the system before the operation with D^0;
- The beam energy requirement has been reduced slightly in DEMO (800 keV versus 1 MeV in ITER) to improve the overall reliability;
- The maximum ion source filling pressure has been decreased, to increase efficiency. In fact, the beam losses in the accelerator are strictly linked to the gas density in the accelerator, that in turn is proportional to the pressure in the ion source;

- The maximum divergence of the beamlets must be very small in both cases; this is required for an optimal optics of the neutral beam, allowing a large fraction of the particles to reach the plasma inside the main chamber;
- The required accelerated current has been decreased, to increase availability of the NBI at the required level of performance;
- The extracted e^-/D^- fraction (or e^-/H^- fraction if the operations are with hydrogen ions) must be in both experiments kept lower than 1. A low ratio permits to limit the heat loads on the extraction grid (EG) and to increase the efficiency of the extraction/acceleration system, but can be obtained only with a good conditioning of the ion source;
- A neutralization efficiency higher than 0.7 has been introduced as a requirement of the DEMO NBI, because it is one of the main tools to decrease the recirculating power. On the other hand, neutralization efficiency is not a requirement for the ITER NBI;
- The beam-on time is doubled with respect to ITER (two hours instead of one hour), to cope with DEMO requirements in terms of long pulse ($>$ 2h) operations.

	ITER NBI	DEMO NBI
Extracted current density (Am^{-2})	293	200
Aperture radius (m)	0.007	0.007
Number of aperture columns per source	20	4
Number of aperture rows per source	64	15
Number of sub-source	1	20
Total extraction area (m^2)	0.197	0.185
Extracted current (A)	57.7	36.9
Acceleration voltage (kV)	1000	800
Auxiliaries/extraction overall efficiency	0.9	0.9
Gross power (MW)	64.1	32.8
Stripping/halo current losses efficiency	0.7	0.9
Accelerated current (A)	40	33.3
Beam source transmission efficiency	0.95	0.98
Neutraliser efficiency	0.55	0.7
Beam line/duct transmission efficiency	0.8	0.92
Power released to the plasma (MW)	16.7	16.8
Injector overall efficiency	0.26	0.51
Number of injectors	3	3
Overall NBI power to the plasma (MW)	50.1	50.4

DEMO is actually in the conceptual design phase, so the efficiency is only an approximation and the RAMI approach is only a guideline for the development of the design.

Recovery system

2.1 Previous studies

The energy recovery system developed by J.Pamela and S.Laffite could be used on deuterium beams with energy around 1 MeV. On these injectors, a major difficulty will consist in the high-voltage power supplies (HVPS) that have a big weight on the cost of injectors, maybe as large as 50%. For this reason the main goal is to produce neutral beam with the highest possible energy.
The recovery process is based on an electrostatic separation carried out by a deflector which separates positive and negative ions and done this the first ones are dumped at full energy or eventually decelerated and the second ones are decelerated. The deflector is made of baffles in order to reduce the gas pressure and trap secondary electron by an electric field. The unneutralised beam ions are collected on a lower-voltage electrode and to prevent thereby the corresponding current to be drained from the HPVS.
Two of the most important features of this model are simplicity in implementation and economy, since no additional power supplies would be required. This solution can have an efficiency around 60%, plus energy recovery systems. There is also another advantage that is the reduction of the residual ion beam power that has to be dumped before neutral beam enters in magnetic field.

2.1.1 Difficulties

In their studies they underline three difficulties *that severely constrain the choice of an energy recovery scheme* like the one wich we talk about. This difficulties are:

1. Energetic D^+ and D^- ions are present at the exit of the gas neutraliser;
2. The cross section for D^- stripping is large. Therefore pressure has to be reduced in the recovery system;
3. Secondary electron emission from the negative ion collector has to be suppressed.

The main reactions that occur when a negative D^- ion beam passes through a gas neutraliser are :

1. Stripping: $\underline{D}^- + D_2 \rightarrow \underline{D}^0 + e + D_2$;
2. Ionisation of D^0: $\underline{D}^0 + D_2 \rightarrow \underline{D}^+ + e + D_2$;
3. Charge exchange: $\underline{D}^+ + D_2 \rightarrow \underline{D}^0 + D_2^+$.

in which beam particles are underlined.

2.1.2 Beam composition

The fraction F of positive, negative and neutral ions depend on the gas target thickness nl, an example is shown in the following figure:

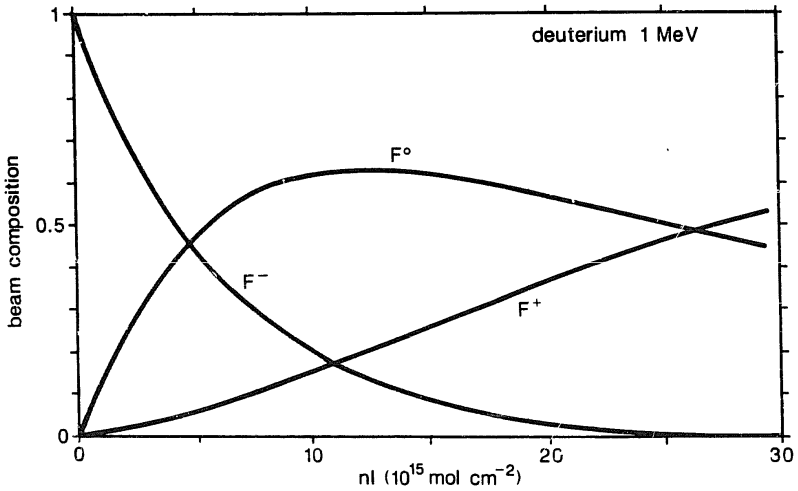

Figure 2.8: Beam composition of a 1 Mev deuterium beam as function of gas target thickness.

We can see that operation at low gas target thickness (around $nl \approx 6 \times 10^{15}$ mol cm^{-2}) would be very favourable for energy recovery and in this conditions F^- is four time larger than F^+, for this reason, in their project, Pamela and Laffite didn't provide recovery of positive ions, because this might complicate the injector design and operation. For the deflection of negative and positive ions they used an asymmetric (for a better separation of ions) deflector purely electrostatic. They wrote that a magnetic deflection is also possible, but also that it can be difficult because requires large electromagnets surrounded by electrostatic and magnetic shielding.

2.1.3 Expected results

The 15% cost reduction is an upper limit of the benefit that can be obtained with this system and is equivalent to using a fully ionised plasma neutraliser with 85% neutralisation efficiency. The most important parameter is the efficiency ϵ_r with which the unneutralised negative ion current is recovered, this parameter has to be larger than 0.8 if we want an useful energy recovery. Efficiency depends, in first approximation, on the thickness of the residual gas in the recovery device ($P_0 L$) and on the effective secondary emission coefficient of negative ions collector (γ_c^*) which must be much lower than 1. In formulas:

$$\epsilon_r \approx (1 - kP_0L)(1 - \gamma_c^*) \tag{2.1}$$

Where k is a term proportional to cross section of stripping power and ionization, P_0 is the mean pressure of residual gas along the ion path from the deflection region to the collector and L is the length of this path. With an efficient gas evacuation an efficiency of 0.9 can be obtained.

2.1.4 Geometry

The geometry of this project was built taking into account the electrical and spatial characteristics of the beam. Polarizations of electrodes were chosen to deflect the ions and decelerate the negative ones and to collect at full power the positive ones, in fact they choose not to decelerate positive ions to avoid technical difficulties. The recovery system is based on following aspects:

1. The residual positive and negative ions are electrostatically separated;
2. the electrostatic deflector is made of baffles (eventually be alternatively polarised) in order to reduce the gas pressure and trap the secondary electrons by an electric field;

3. the negative ions are decelerated and the positive ions are dumped at full energy or eventually decelerated;
4. the decelerated negative ions are collected on a composite electrode acting as an electrostatic trap for secondary electrons.

In figure 2.9 we can see a two-dimensional simulation that they do using the SLAC code:

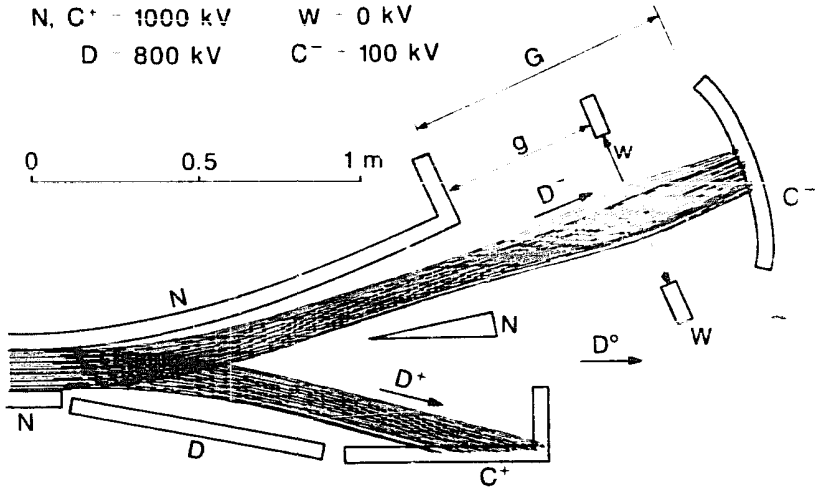

Figure 2.9: SLAC simulation.

where C^+ and C^- are collectors of positive and negative ions respectively, D is the deflector and W is the window that is polarized negatively with respect to C^- and does not intercept the decelerated ions. This is intended to prevent electron emission from the surface to the collector. Trajectory calculations shows that W can be polarised at -V_B with respect to the neutraliser.

The separation of positive and negative ions occurs through an electrode negatively polarized with respect to the neutraliser, this is fundamental because, in the opposite case, beam plasma electrons and secondary electrons created on C^+ or on other components held at neutraliser potential would be accelerated onto the deflector electrode. The angle of deflection is given by the following formula:

$$\alpha = \arctan\left(\frac{\Delta V L_d}{2V_B W_d}\right) \tag{2.2}$$

where V_B is the beam accelerating potential, ΔV is the drop of potential from neutraliser to deflector, W_d and L_d are width and length of deflector. For the choice of parameters is important to try to use potentials already available in order to reduce costs and a short L_d to reduce beam-gas deleterious effect. In their project α is about 15°.

When positive ions are collected on C^+ and, if the collector is at the same voltage as the neutraliser, it happens at full power, without deceleration. Collector is loaded with the following average power density:

$$p = \frac{F^+ I_{acc} V_B}{H_B W_B} \sin\alpha \tag{2.3}$$

where I_{acc} is the accelerated D^- current and W_B and H_B are the beam width and height. With the parameters of their project the average power density would be around 100 W/cm^2 with peaks of 300 W/cm^2, it can be reduced with baffles or increasing of C^+ voltage.
D^- ions drift in a equipotential space before being decelerated that has to be as short as possible, in order to reduce losses by stripping. After the drift tube a decelerating electric field is applied to recover D^- ion current on a low-voltage electrode. The efficiency of recovery is related to the deceleration factor δ:

$$\delta = \frac{E_r}{E_B} \tag{2.4}$$

where E_r is the energy in the recovery system and E_B the full beam energy. In the case of the simulation in figure (2.9) $\delta = 0.1$, but calculation shown that also low values as 0.05 can be obtained. They solved Laplace and Poisson equations in various cases and they obtained the following relation between dimensional parameters of collector and decelerator (see figure 2.9):

$$G \geq g + k(\delta)w \tag{2.5}$$

where $\gamma_c^* = 0$, k(δ) is a decreasing function of the decelerating factor δ (for example if δ= 0.05-0.1-0.2 k(δ) = 1.5-1-0.6). This relation in independent from V_B.

2.1.5 Results obtained for a powerful 100 keV D^- based neutral beam injector

In the studies after 1990 they adapted the recovery system to powerful 100 keV D^- based neutral beam injector and they developed the final project shown in the following figure:

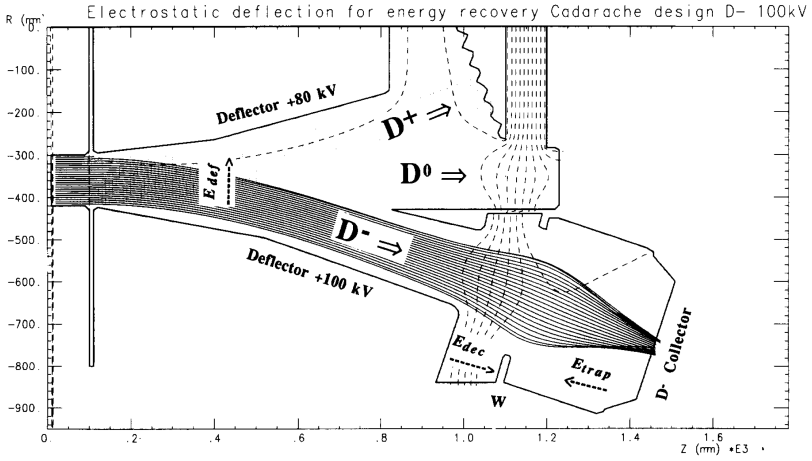

Figure 2.10: J.Pamela and S.Laffite project (1992).

Energy recovery system consists of decelerating the residual unneutralized beam ions and collecting them at a potential lower than that of electrostatic accelerator. RPS(recovery power supply) drains the current of this ions instead of being taken from the main accelerating high voltage power supply (HPVS).
Below the electrical schemes of the two cases are reported:

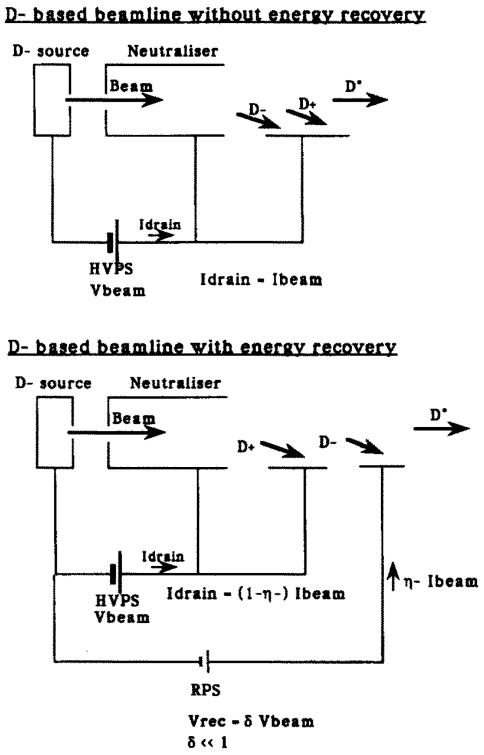

Figure 2.11: Principle of energy recovery on negative ion based neutral beam lines.

In the first case the HPVS drain current I_{drain} corresponds (approximately) to the total accelerated beam current I_{beam}. Using RPS drains a current I_{rec} that is a fraction ϵ(efficiency of collection) of the unneutralized negative ion current I_-:

$$I_{rec} = \epsilon I_- = I_{drain} F^- I_{beam} \tag{2.6}$$

in this case the HPVS drain current is

$$I^*_{drain} = I_{beam} - I_{rec} = I_{beam}(1 - \epsilon F^-) \tag{2.7}$$

Redefining now the deceleration factor:

$$\delta = \frac{V_{rec}}{V_{beam}} \tag{2.8}$$

the efficiency of energy recovery system $\mathcal{E}$, which measures the fraction of residual negative ion power saved, depends on the previous parameters and in the ideal case (without additional power consumption) is:

$$\mathcal{E} = (V_{beam} - V_{rec}) I_{rec} / V_{beam} I_- = (1 - \delta)\epsilon \tag{2.9}$$

To maximize this parameter geometry has to be carefully designed in order to yield a low $\delta \approx 0.05 - 0.1$ and a maximum ϵ. Problems in this project are the same of previous one, so this purely electrostatic system has been designed to accomplish several tasks:

1. To **separate** the neutral and charged components of the beam at the exit of gas neutraliser.
   A transverse electric field E_{def} is applied between two electrodes placed on the either side of the beam. The positive and negative ions are deflected in opposite direction, toward separate target electrodes (collectors);

2. To **decelerate** the residual unneutralised negative ions.
   An electric field E_{dec} is applied between the exit of deflector and negative ion collector;

3. To **prevent** secondary emission of electrons from the negative ion collector.
   A third electrostatic field, E_{trap}, is applied on the surface of collector. This is simply supplied by the frame W.

4. To **operate** at low pressure.
   Therefore gas pumping is applied both at the exit of the neutraliser and inside the electrostatic deflector.

An energy recovery system based on the previous concepts has been constructed by the EU-RATOM-CEA Association and has been tested in the framework of the joint EURATOM-CEA/JAERI experiment conduced at Cadarache from April 1991 to April 1992 (figure 2.12).

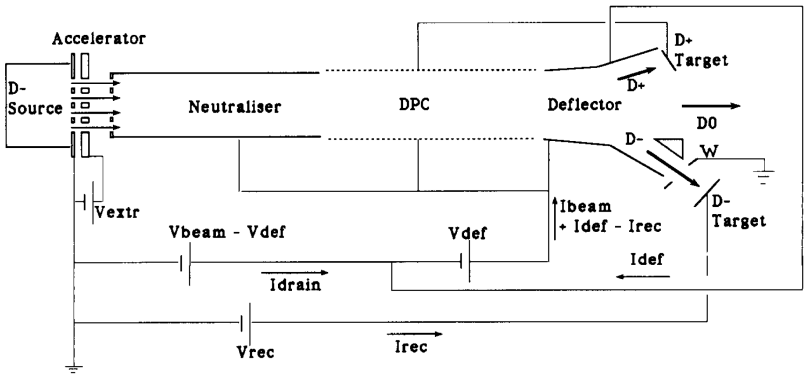

Figure 2.12: Scheme of the beam line with the electrical circuit.

where DPC is a differential pumping chamber. I will not discuss the experiment in detail because, as you will see in the following chapters, the same values for potentials will not be used, but it is important to stress the fact that yield $\mathcal{E}$ obtained was 81%. The work done by Pamela and Leffite will serve as starting point.

Optimization of the project

Starting from the project just discussed, we now move on to the proposal of three different energy recovery solutions:

1. Electrostatic deflection with negative ions recovery (EN);
2. Electrostatic deflection with positive and negative ions recovery (EPN);
3. Magnetic deflection with positive and negative ions recovery (MPN).

Before discussing the proposed solutions we will see the context in which the apparatus must be inserted, and therefore the structural and energy characteristics to which it must be adapted. We will also briefly review the software used for simulations.

3.1 DEMO NBI

Controlled nuclear fusion uses high power neutral beams to bring the plasma to high temperatures. Ion sources used in DEMO are characterized by high energies (800 keV) and currents (several hundred keV) and consequently by high powers (several tens of MW). DEMO NBI is composed of the following part:

- A negative ion beam source, composed of 20 sub-sources (two adjacent columns of 10 sub-sources each);
- A PN based on the (RING) concept, but compatible with other options;
- A residual ion dump (RID) featuring a flat water-cooled CuCrZr plate. It is foreseen to work with a magnetic deflection of the residual ions generated by the stray field by the Tokamak coils. In fact, this field should be sufficient to deflect the residual ions onto the RID plate or onto the two duct heat dumps located downstream of it. As an alternative, a proper source of magnetic or electric field could be added in the in RID region to deflect the residual ions (topic of this thesis);
- A beam source vessel, containing the entire beam source with the related NEG pumps;
- A beam line vessel, containing the complete neutraliser and RID structures;
- A duct connecting the beam line vessel to the Tokamak chamber. The duct features a large NEG pump (to reduce gas density and re-ionization losses) and two heat dumps (to dump the heat loads by re-ionization).

Conceptual design is in fact designed to be substituted for the RID (figure 3.14) contained in the DEMO neutral injector (Figure 3.13).

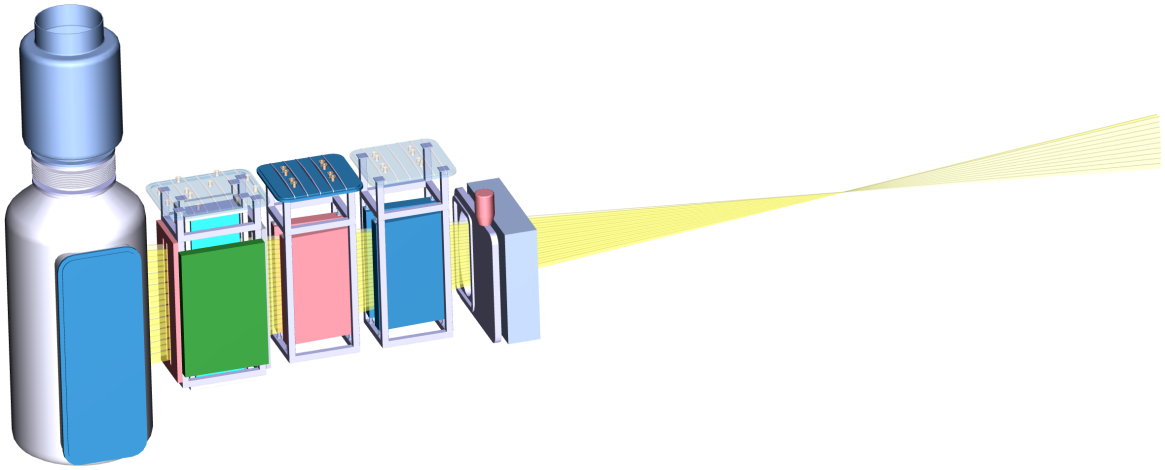

Figure 3.13: DEMO injector without vessel.

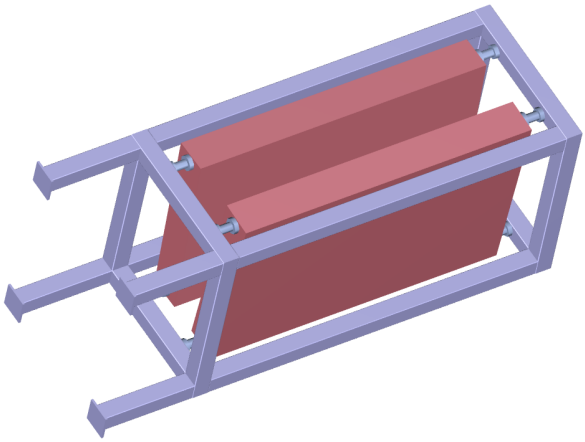

Figure 3.14: DEMO RID.

Current configuration is not designed for ion recovery, but only to absorb them so as to inject only neutral ions.
The dimensions of the RID without support are as follows:

Width (m)	3.50
Height (m)	2.15
Thickness (m)	1.33

The RID is contained in a metallic vessel shown in the following figure:

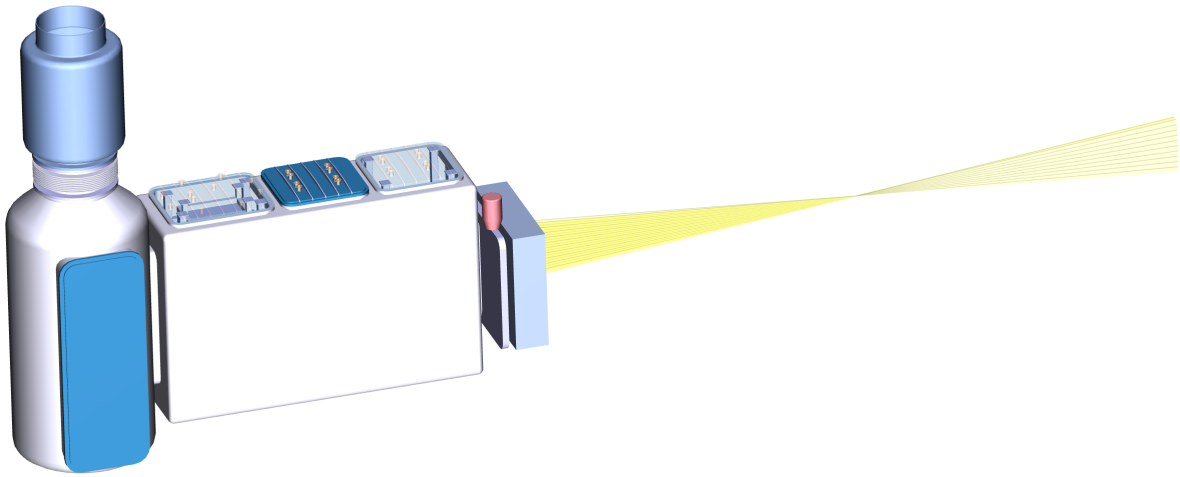

Figure 3.15: DEMO injector.

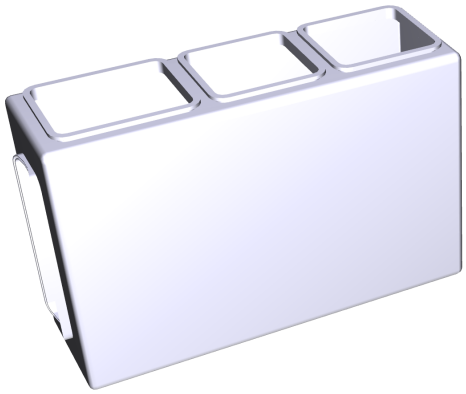

Figure 3.16: DEMO vessel.

The measurements of the upper part of the second cavity, on which the coils (for MPN) are to be positioned are:

Basis (m)	2.4
Height (m)	2.3

and the height measured in the direction perpendicular to this cavity is about 6 m.

3.2 COMSOL Multiphysics

In mathematics, the finite element method (FEM, Finite Element Method) is a numerical technique designed to look for approximate solutions of problems described by differential equations to partial derivatives, reducing them to a system of algebraic equations. COMSOL Multiphysics is a module-structured finite elements code, featuring a wide variety of separate "Physics Modules" (such as Electrostatics, Structural Mechanics, Heat Transfer, and many more) that can be added to a model to simulate "multi-physics" problems and interaction between different parameters. As an addition,

the software has a choice of different solvers, in relation to the problem at hand. As an example, the AC/DC module simulate a current in a conductor and see its displacement; if the Heat Transfer is added, the Joule effect can be evaluated, and finally by adding the Structural Mechanics the thermal stress on the conductor can be obtained; all of them can be computed imagining a stationary situation, or with a time-dependent function. This great versatility makes COMSOL a perfect choice for the study of a complex system like the DEMO accelerator, where the electrostatic, magnetic and particle tracing aspects must be evaluated at the same time; as a drawback in comparison to dedicated codes though (like EAMCC, SLACCAD, AVOCADO, etc., each one with its area of expertise) the convergence of model solution can be hard to obtain, especially with large multiphysics models or weak boundary conditions; secondly, for modules like the Particle Tracing, the FEM approach it is not the best one unless the model mesh is carefully chosen.
For these kind of analysis COMSOL offers a preset physics and study assembly, called the Particle Field Interaction, non relativistic: basically, once the model and boundary condition are input, COMSOL engages in a multi-iterative step process solving first the electric and magnetic static fields (comprised with the particle space charge contribution):

$$\nabla^2 V = -\frac{\rho}{\varepsilon_0} \tag{3.10}$$

$$\vec{\nabla} V_m = -\vec{H} \tag{3.11}$$

$$\nabla \cdot \vec{B} = 0 \tag{3.12}$$

After the static field has been computed, the code uses a time solver to plot the particle trajectories under the generalized Lorentz force:

$$m_i \frac{\partial^2 \vec{x_i}}{\partial t^2} = q_i(\vec{\nabla} V + \frac{\partial \vec{x_i}}{\partial t} \times \vec{B}) \tag{3.13}$$

Where the i-es quantities are referred to the particle and B is the applied magnetic field. The process repeats for a user-specified number of iterations, until convergence is achieved: such number will be determined with a separate sensibility analysis.
The Magnetic Fields (mf) interface , found under the AC/DC branch when adding a physics interface, is used to compute magnetic field and induced current distributions in and around coils, conductors, and magnets. The function Multi-turn coil use this equation and boundary conditions for a stationary study of magnetic field:

$$\vec{J_e} = \frac{N I_{coil}}{S} \vec{e_{coil}} \tag{3.14}$$

$$\nabla \times \vec{H} = \vec{J} \tag{3.15}$$

$$\nabla \times \vec{A} = \vec{B} \tag{3.16}$$

$$\vec{J} = \sigma \vec{E} \tag{3.17}$$

$$\vec{n} \times \vec{A} = 0 \tag{3.18}$$

where e_{coil} is the local direction of the coil, S is the section, N is the turns number, I_{coil} is current that flows through into the coil and σ is the superficial charge density.

3.3 Analytical verification

Before continuing with the analysis in FEM, we report analytical accounts in order to have an element of comparison for the results of COMSOL.

3.3.1 Particle velocity EPN

In this configuration ions are affected by the deflector's potential (175 kV) and change their direction under the effect of Lorentz force. At the beginning of trajectory they reach the maximum speed, which is then reduced in the final part of the apparatus containing windows and collectors kept at specially calibrated potentials. This speed can be obtained from the kinetic energy of the particle:

$$v_0 = \sqrt{\frac{2E}{m}} \tag{3.19}$$

Using the following values:

q (C)	1.602176×10^{-19}
E (keV)	800
m_p (kg)	1.672621×10^{-27}

result $v_0 = 8.8 \times 10^6$ (ms^{-1}) which is compatible with that obtained from the analysis of trajectories performed for EPN in the simplest case (disabled windows) (figure 3.24) of 9.3×10^6 (ms^{-1}) .The other potentials certainly influence the velocity of the particles, but the result obtained allows the analysis in COMSOL to be considered valid.

3.3.2 Deflection EPN

We can approximate the electric field with that of a uniformly charged infinite plane with charge density σ and, having set the electric potential V to -175 kV we can obtain this density in order to get the electric field, to calculate the Lorentz force and therefore the acceleration of particles. In formulas:

$$V = -\frac{\sigma d}{2\epsilon_{air}} \Rightarrow \sigma = \frac{-2\epsilon_{air} V}{d} \tag{3.20}$$

$$E = \frac{\sigma}{2\epsilon_{air}} = \frac{V}{d} \tag{3.21}$$

$$F = qE \tag{3.22}$$

$$F = ma \Rightarrow a = \frac{F}{m} \tag{3.23}$$

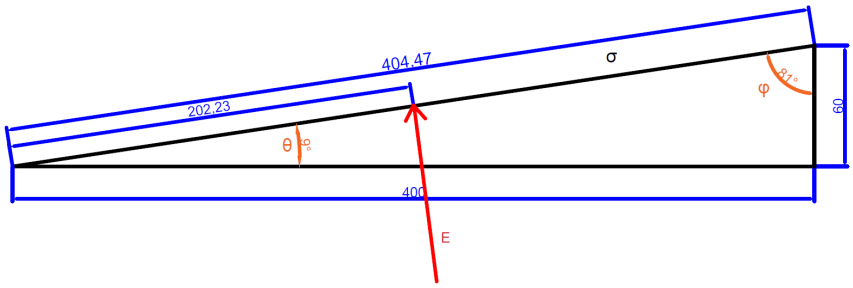

Figure 3.17: Schematization of deflector.

The distance between the midpoint of the hypotenuse and the reflection axis of the collector geometry is obtained from simple trigonometric computations and results $d = 106$ (mm). Electric field is oriented as in Figure 3.17 and is decomposed into the x and y components:

$$E_x = E \cos\phi \tag{3.24}$$

$$E_y = E\cos\theta \tag{3.25}$$

It is obtained that $E_x = 0.2 \times 10^6$ (Vm^{-1}) and $E_y = 1.63 \times 10^6$ (Vm^{-1}), so we can see that first one is negligible compared to the second (will have a slight braking effect on the particle), for this reason the force exerted by the electric field (3.22) is calculated using only E_y. Imposing $\epsilon_{air} = 8.8542 \times 10^{-12}$ (Fm^{-1}) dielectric constant of air result $a = 7.8 \times 10^{13}$ (ms^{-1}).
With this information we can calculate the equations of motion and compare the trajectory obtained analytically with that of the simulation:

$$\begin{cases} x = v_0 t \\ y = \frac{1}{2} a t^2 \end{cases} \tag{3.26}$$

The trajectories obtained analytically are listed below:

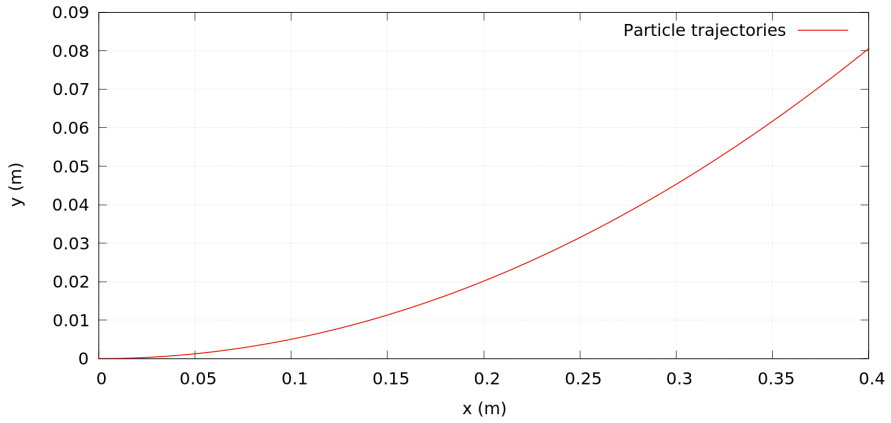

Figure 3.18: Theoretical trajectory.

In the analytical treatment of the problem, only the part of deflector (400 mm) has been considered, since after the particle crosses the initial region where only the deflector potential is present, it suffers the effects of other surfaces maintained at different potentials and which generate complex fields in order to restrain it. Since the purpose of the calculation is to determine if the program works correctly, it is sufficient to calculate the trajectory in the initial journey. The computation was made for positively charged particles, in the case of negative ions the trajectory will be reflected with respect to the x axis. From the figures it is evident that analytical trajectory correspond to the COMSOL one (Figure 3.23) , the differences are due to the fact that we are considering only the field produced by the deflector and that we are neglecting the x-component.

3.3.3 Magnetic field MPN(1)

I analytically analyse the simplest case of MPN studied, ie the one with the windows disabled. Approximating the square-section loop used to generate the magnetic field as a linear square loop, it is possible to calculate the field along the axis passing through the centre, in formulas:

$$B = \frac{\mu_{air} I L^2}{2\pi(z^2 + \frac{L^2}{4})\sqrt{z^2 + \frac{L^2}{2}}}^2 \tag{3.27}$$

[2]Grivich, Am. J. Phys. 68 (2000) 469

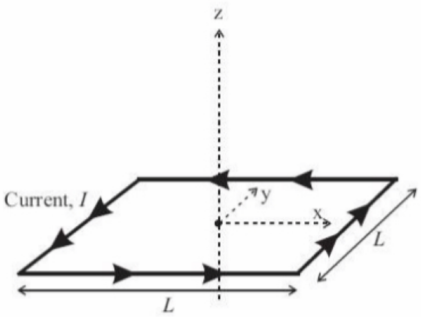

Figure 3.19: Square loop.

Where μ_{air} is magnetic permeability in air (1.2566375×10^{-6} Hm^{-1}), L is the side of coil, I it is the current that circulates there and z is the distance from centre of the loop along the axis passing through it. In the configuration we are dealing with, we have two identical coils positioned along the same axis, so the field obtained with 3.11 is multiplied by two. The parameters of MPN(1) are:

L (m)	2.05
I(A)	5.00×10^5
z(m)	3.00

Where L has been approximated to the average path, since the coil input consists of a square section (figure 3.32) and not a closed line. Using the data in the table we obtain a value of the magnetic field (in module) equal to 2.51×10^{-2} T which is comparable with the value obtained by simulation on COMSOL of 2.41×10^{-2} T. Obviously the difference is due to the fact that it is an approximation, but the result obtained guarantees that the FEM is functioning correctly.

3.3.4 Deflection MPN(1)

Once the field has been calculated, this has been exported to the MPN model and it has been used for particle deflection, to verify that this simulation is correct it is necessary to analytically calculate the deflection of the ions and compare it with the one obtained by COMSOL. A charged particle in a uniform magnetic field moves with uniform circular motion, the idea is therefore to take two points (taken before the windows and collectors, which can remove the behaviour of the particle from the classically expected) of the trajectory obtained by simulation and thus obtain the radius of the circumference and compare it with that obtained analytically with the following formula:

$$R = \frac{mv_0}{qB} \tag{3.28}$$

Where v_0 it is the initial velocity of the particle and is the same of 3.3.1 obtained from kinetic energy, q it is the charge of the particle (in our case $\pm e$), B the magnetic field of two coils and m is the mass (in our case $2m_p$). The radius obtained from 3.12 is therefore R = 3.8 m.

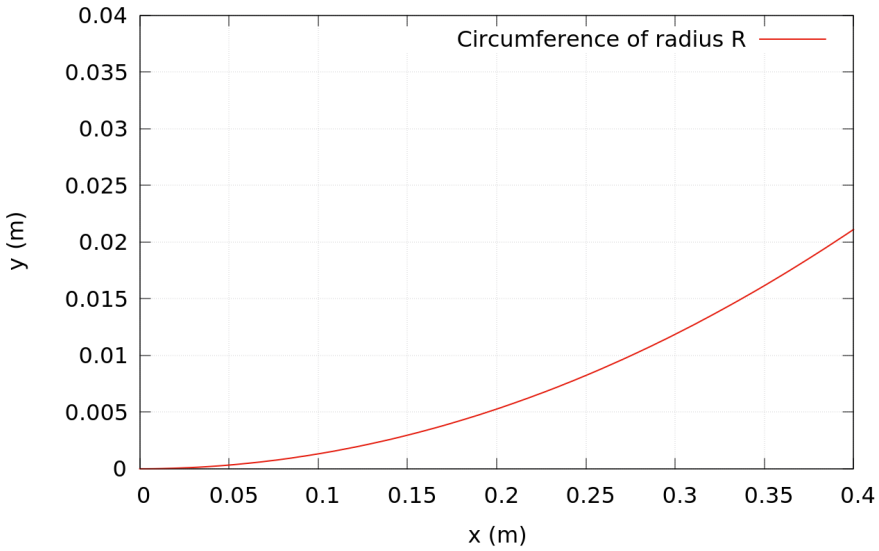

Figure 3.20: Theoretical trajectory

Deflection calculated by COMSOL, in the case of windows disabled (Figure 3.31), is consistent with that calculated analytically.

3.4 Proposed solutions

These three solutions have the same particle injection system. As an entry there is a small section of the surface in which the particles coming from the neutraliser (immediately preceding component) have been considered, in order to remove the beam from the surfaces and avoid to have edge effects during the simulation. The particles injected are:

Particle	Mass	Charge number
D^0	$2m_p$	0
D^+	$2m_p$	1
D^-	$2m_p$	-1

All the geometries we have seen are such as to require a thickness and a width smaller than that of the DEMO RID, the height is exploited entirely to allow the absorption of all the ions of the beam. The proposed geometry for EPN and MPN configurations is shown below:

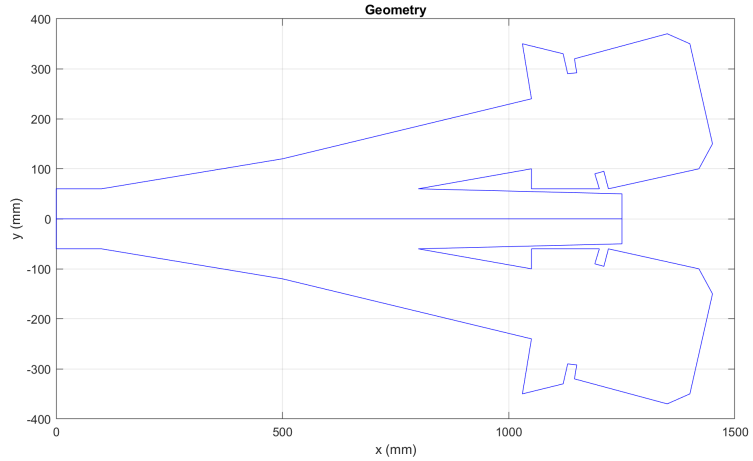

Figure 3.21: 2D proposed geometry.

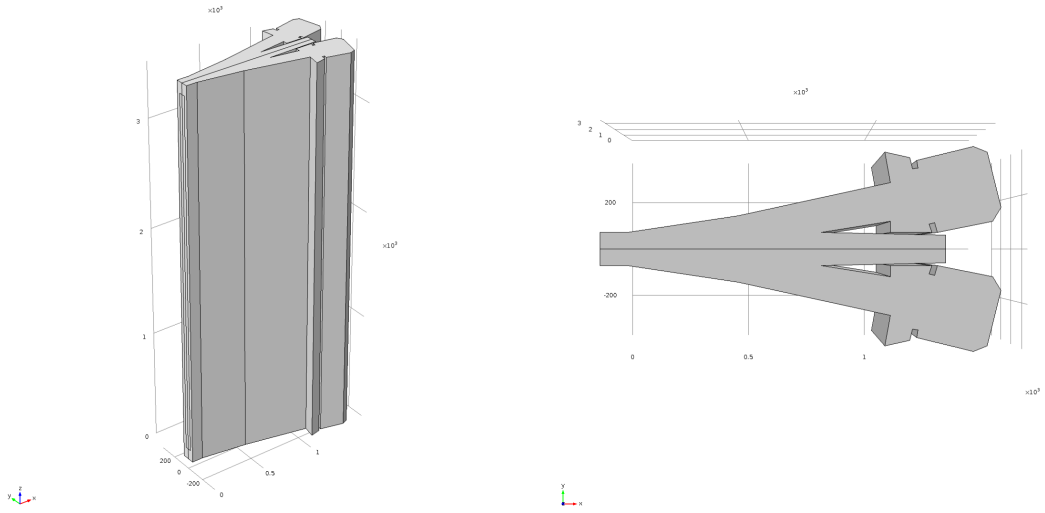

Figure 3.22: 3D proposed geometry (mm).

Despite being turned off the windows are not removed from the geometry, as necessary (as emerges from the simulations in COMSOL) for the braking of ions, indeed it is necessary to generate E_{def}, E_{dec} and E_{trap} discussed in chapter 2.

3.4.1 Electrostatic deflection with negative ions recovery

This is the simplest configuration, which was taken from the original design of J.Pamela and S.Laffite. The only changes are due to the different characteristics of DEMO, in fact the particles in this experiment have an energy of 800 keV and not 1 MeV (value for which the apparatus was calibrated) and also dimensions are different. Apart from these adaptations, the apparatus remains identical to the original one, furthermore, for the types of beams produced it would not be very functional, since these contain both types of ions in comparable quantities; for these reasons I will not treat it as a possible solution for DEMO.

3.4.2 Electrostatic deflection with positive and negative ions recovery

This conceptual design is an optimization of the original one, in fact it foresees that also the negative ions are recovered. The geometry (Figure 3.21 3.22) is a reflection of the positive ions collection apparatus in order to pick also those of opposite sign. The difference with respect to the EN case, which is important to discuss, is the function of windows, in fact in the main configuration these were intended to enlarge the beam to reduce the thermal load (Figure 2.10), but in new geometry you can see that if you consider a symmetrical situation in which the two windows have equal charge in module (800kV), the thermal load is not the same on two collectors (Figure 3.24) , this is probably because the situation is not actually completely symmetrical, in fact only one deflector with negative charge is used (-175 kV) and therefore the negative charges undergo further acceleration, for this reason a third case, in addition to the two in which the windows are simply enabled or disabled, is also considered. From the simulations made in COMSOL it emerges that, in this set-up, small variations from symmetry, as regards the potentials, have clear effects on the trajectories and on the velocity of particles, for this reason the two windows can not have potentials that differ excessively in the form.

In the following graphs three situations are presented:

1. Activated windows with same voltage in module;
2. Disabled windows(0 kV);
3. Activated windows with different voltage (-500 kV and 800 kV).

Third case is the best configuration that has been found in the case of different potentials for the two windows, in fact several tests have been carried out and the one with the best symmetry regarding heat loads on the two collectors has been chosen.
The results obtained in the three cases, through simulation on COMSOL, are reported below:

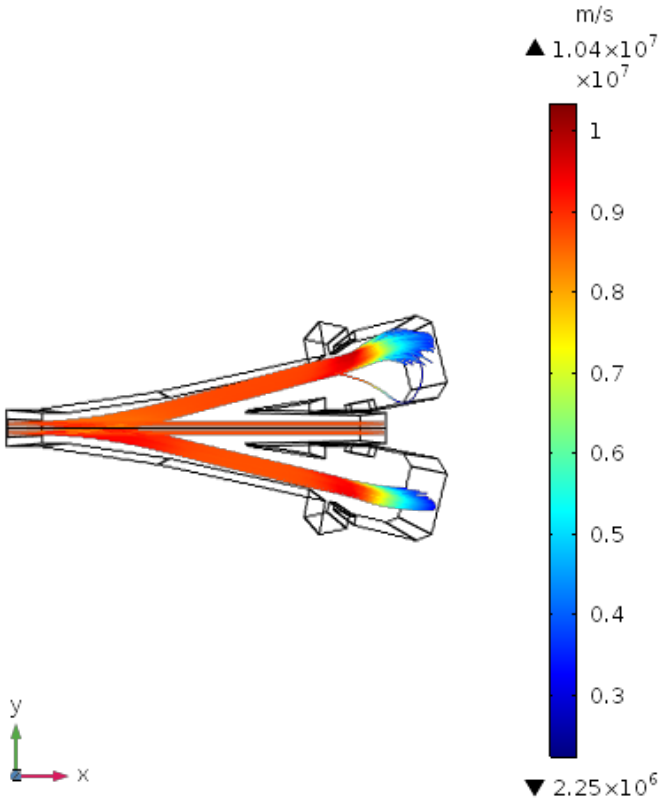

Figure 3.23: Trajectories case 1.

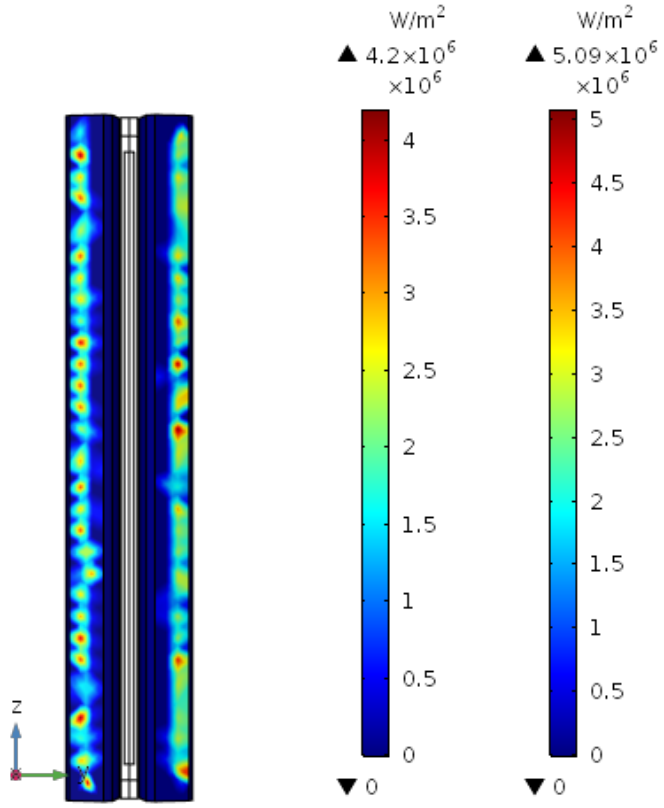

Figure 3.24: Thermal load case 1.

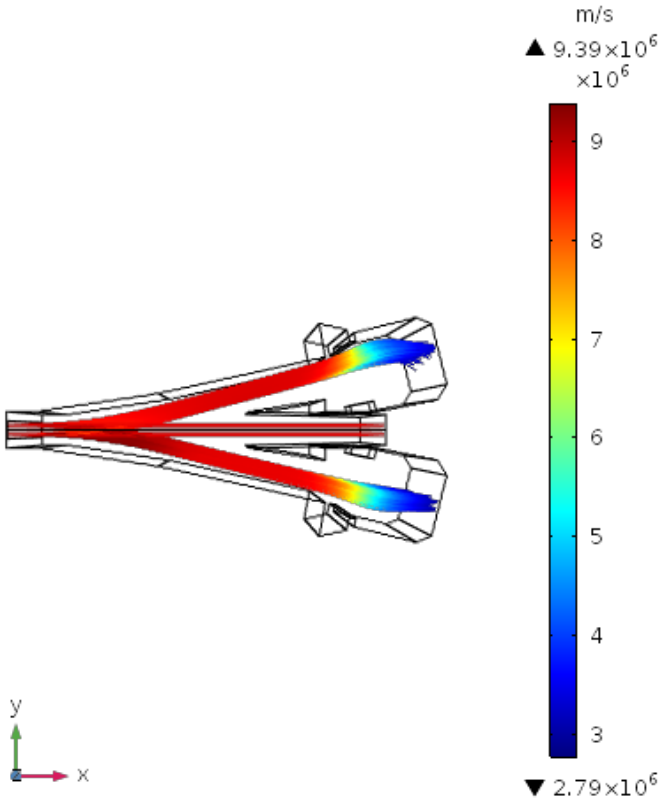

Figure 3.25: Trajectories case 2.

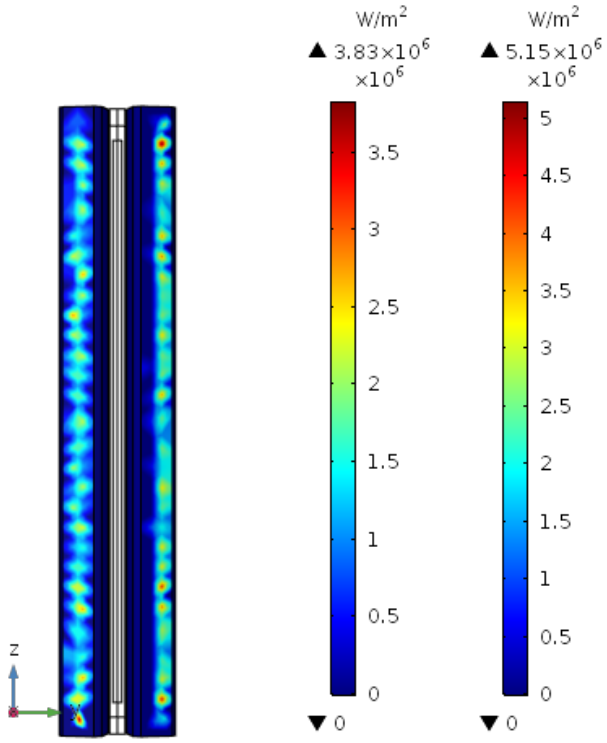

Figure 3.26: Thermal load case 2.

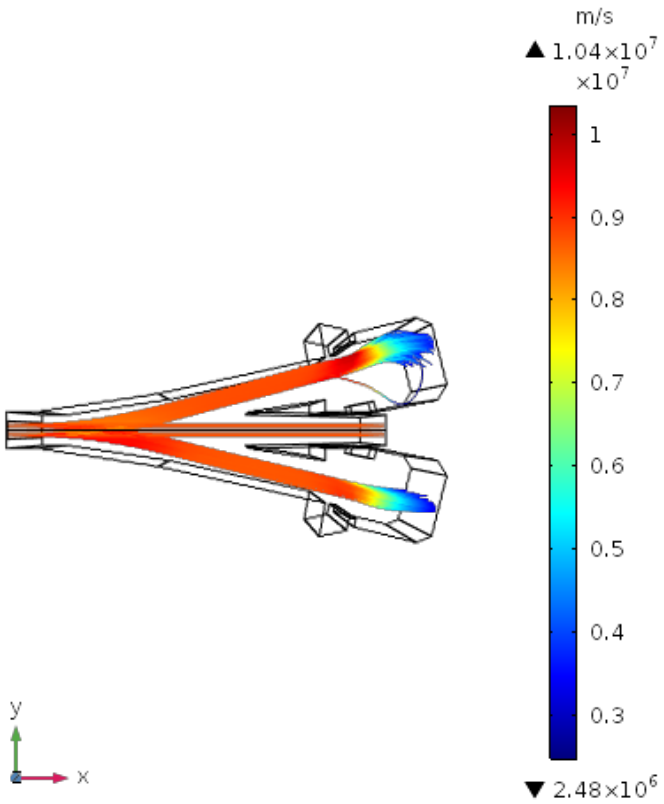

Figure 3.27: Trajectories case 3.

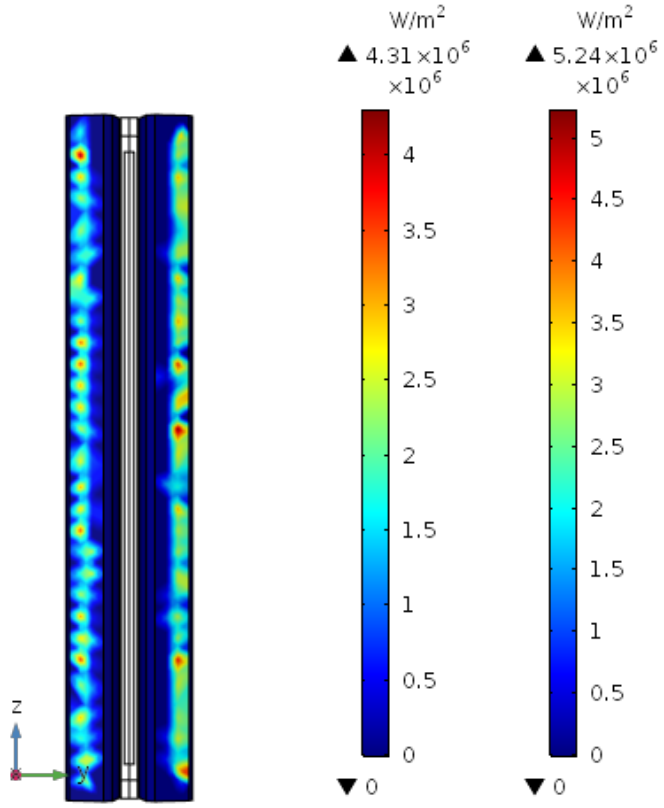

Figure 3.28: Thermal load case 3.

Figures 3.23, 3.25 and 3.27 show the trajectories of ions inside the apparatus, colour scale indicates their velocity which results to be maximum in the initial area (red) and decreases in the proximity of the collectors (blue). Thermal loads are visible in the figures 3.24, 3.26 and 3.28 where, always through a colour scale, the warmest areas are visible, ie those where the particles are most impacted, in the centre of collectors and the colder ones (dark blue) on the margins. Considering now thermal load, the trajectory of particles and the difficulty of realization of the three cases for choosing the best configuration. From the simulations in COMSOL the following data are obtained:

- **Case 1**:
  Maximum velocity 1.04×10^7 (ms^{-1})
  Minimum velocity 2.25×10^6 (ms^{-1})
  Maximum thermal load C^+ 5.09×10^6 (Wm^{-2})
  Maximum thermal load C^- 4.2×10^6 (Wm^{-2})

- **Case 2**:
  Maximum velocity 9.39×10^6 (ms^{-1})
  Minimum velocity 2.79×10^6 (ms^{-1})
  Maximum thermal load C^+ 5.15×10^6 (Wm^{-2})
  Maximum thermal load C^- 3.83×10^6 (Wm^{-2})

- **Case 3**:
  Maximum velocity 1.04×10^7 (ms^{-1})
  Minimum velocity 2.48×10^6 (ms^{-1})
  Maximum thermal load C^+ 5.24×10^6 (Wm^{-2})
  Maximum thermal load C^- 4.31×10^6 (Wm^{-2})

Where C^+ and C^- are positive and negative collectors of ions respectively.
It is evident that the first case turns out to be the worst among three because, as seen in the picture 3.2, there are more areas with a high heat load (red areas). As regards case 3 the asymmetry of potentials guarantees a better symmetry with regard to the thermal loads, but these are still greater than in case 2 for this reasons the latter has been chosen as final solution, considering also the fact that return of ions in cases 1 and 3 (Figure 3.27) that reduces the efficiency of apparatus and could lead to its overheating with the passage of time. From the point of view of the ease of implementation, the second case remains the best since it is not necessary to keep the windows at a potential different from that of environment (0 kV).
Below the potential lines of the final configuration:

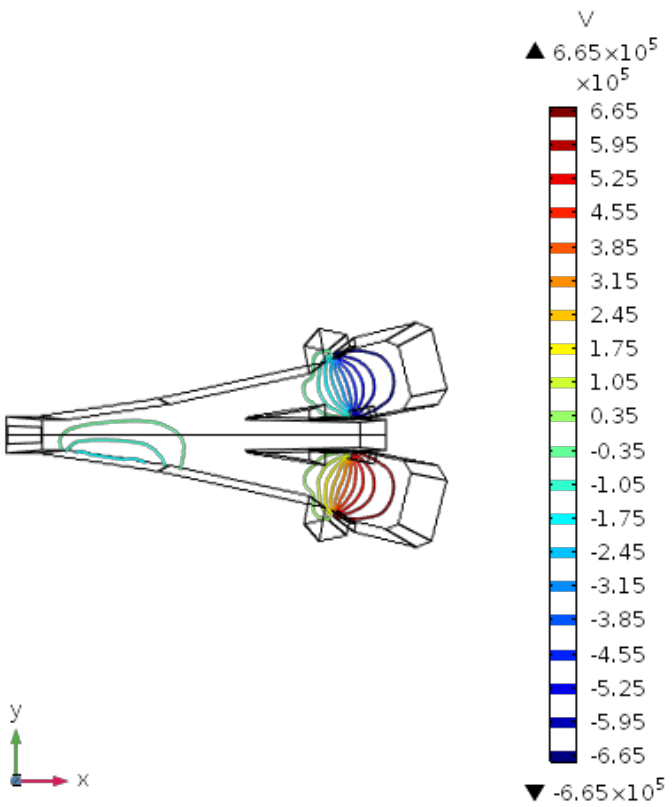

Figure 3.29: Potential case 2.

Let's see the difference between electrical potentials, expressed in (kV), used for EPN (2) and for J.Pamela and S.Laffite project:

Experiment	EPN	J.Pamela and S.Laffite project
Environment	0	1000
Positive ions collector	700	/
Negative ions collector	-700	100
Negative ions window	0	0
Postive ions window	0	0
Deflector	-175	800

We see that the model is needed, for the power supply, about 1575 kV against 1900 kV of the original configuration. Therefore, in line with the principles of RAMI consumption has been reduced in order to increase the efficiency of the experiment.

3.4.3 Magnetic deflection with positive and negative ions recovery

This configuration in based on magnetic deflection of positive and negative ions. It is now realised through a coil which has been chosen to generate a magnetic field that is as uniform as possible and which we will discuss in detail in the next chapter. The geometry of this configuration is the same as EPN (Figure 3.21 3.22). In Figure 3.30 we can see lines of electrical potential, that are used to stop the ions as much as possible before the impact with collectors. The red area corresponds to a positive potential of about 800 kV and the blue area to a negative one of the same value.

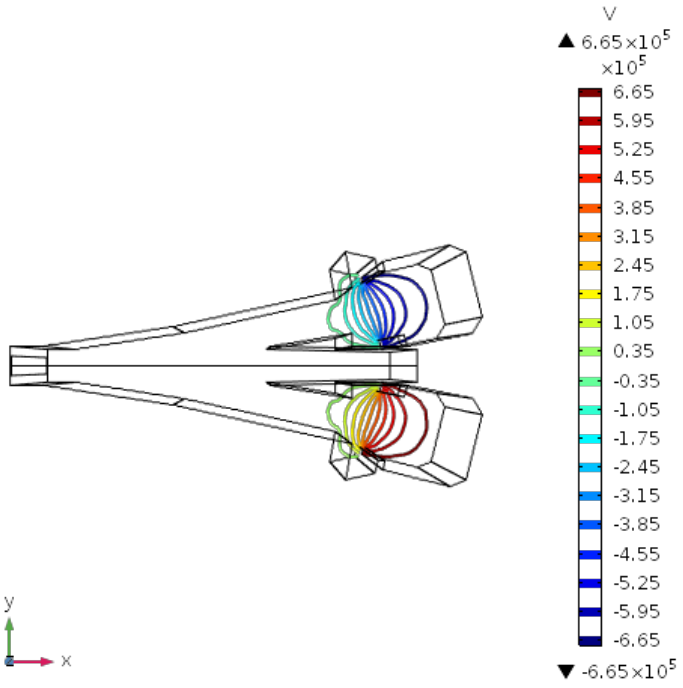

Figure 3.30: Potential MPN.

In this case we can choose whether to keep the windows on. Therefore we have two configurations:

1. Disabled windows with current of coils of 50 kA.
2. Enabled windows (650 kV) with current of coils of 45 kA;

In the second case the choice of the potential for the windows was determined by carrying out test simulations and choosing the optimal one. Compare the two cases:

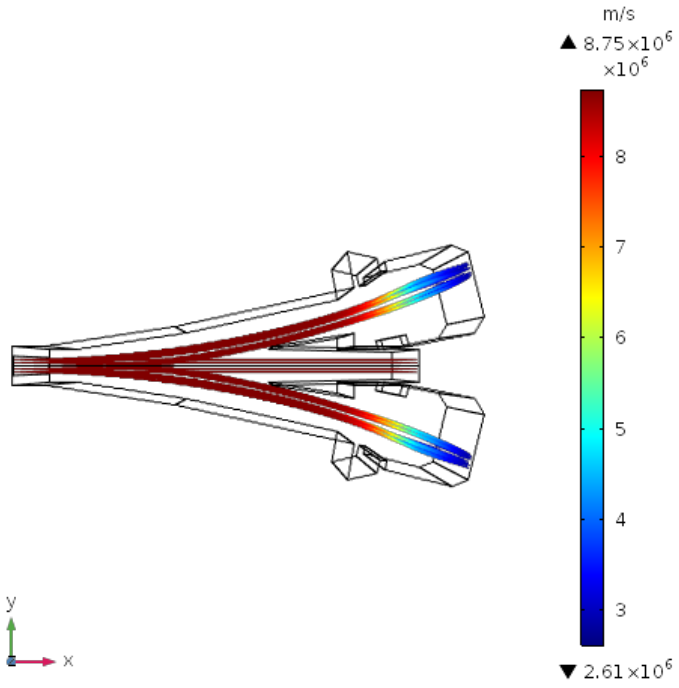

Figure 3.31: Trajectories case 1.

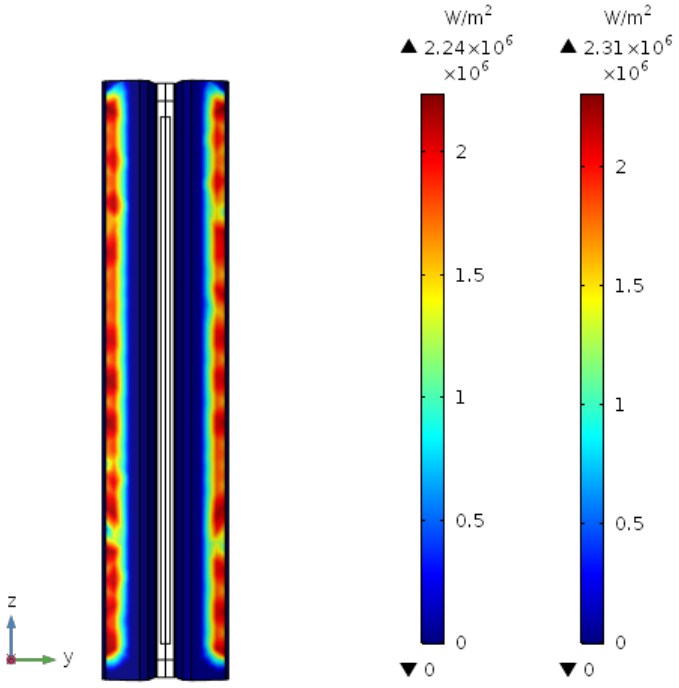

Figure 3.32: Thermal load case 1.

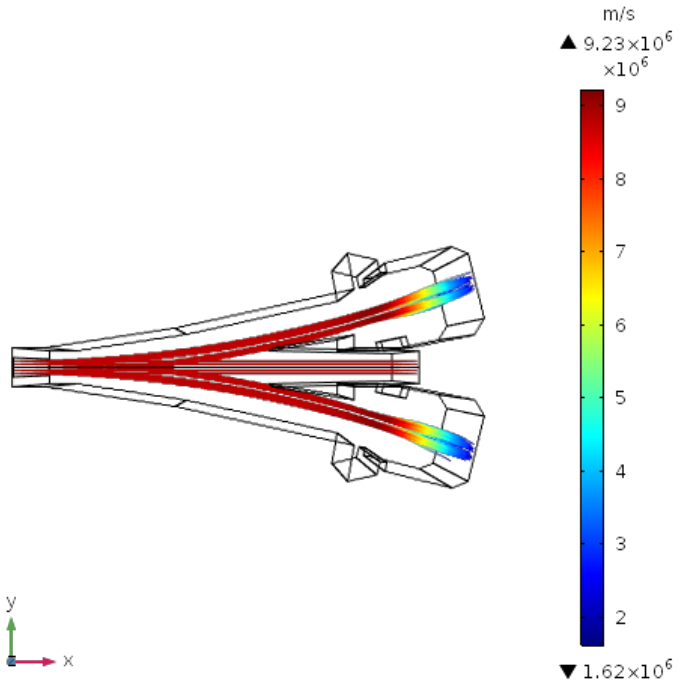

Figure 3.33: Trajectories case 2.

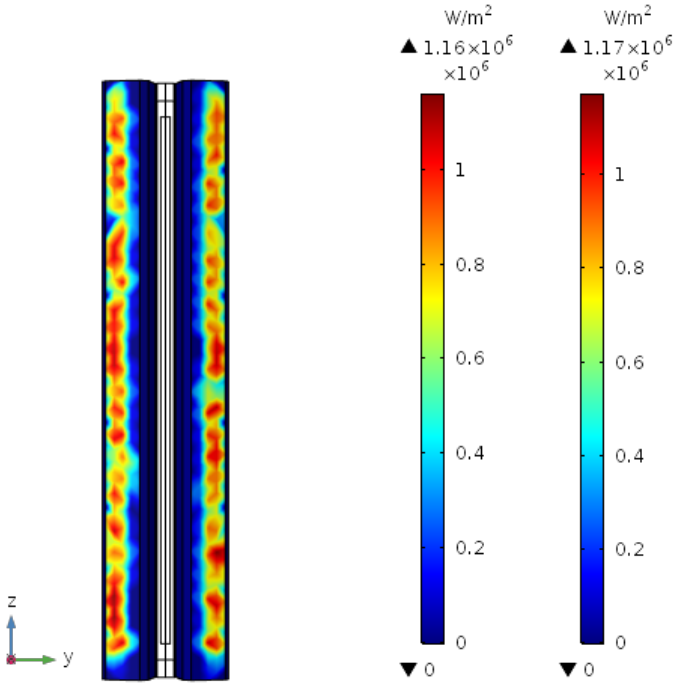

Figure 3.34: Thermal load case 2.

Considering now thermal load, the trajectory of particles and the difficulty of realization of the three cases for choosing the best configuration. From the simulations in COMSOL the following data are obtained:

- **Case 1**:
  Maximum velocity 8.75×10^6 (ms^{-1})

Minimum velocity 2.61×10^6 (ms^{-1})
Maximum thermal load C^+ 2.31×10^6 (Wm^{-2})
Maximum thermal load C^- 2.24×10^6 (Wm^{-2})

- **Case 2**:
  Maximum velocity 9.23×10^6 (ms^{-1})
  Minimum velocity 1.62×10^6 (ms^{-1})
  Maximum thermal load C^+ 1.17×10^6 (Wm^{-2})
  Maximum thermal load C^- 1.16×10^6 (Wm^{-2})

Where C^+ and C^- are positive and negative collectors of ions respectively.
We see that the configuration 2 is the one that gives us the best thermal load not only with regard to the maximum value, but also for the distribution of zones with the highest temperature (red areas) on the collectors, in fact the latter are smaller in number and more distributed than in case 1, as shown by comparing Figures 3.32 and 3.34. Nevertheless the 1 presents a greater ease of implementation, so we consider both valid solutions.
Let's see the difference between electrical potentials, expressed in (kV), used for MPN (2) and for J.Pamela and S.Laffite project:

Experiment	EPN	J.Pamela and S.Laffite project
Environment	0	1000
Positive ions collector	700	/
Negative ions collector	-700	100
Negative ions window	-650	0
Positive ions window	650	0
Deflector	0	800

The potentials used are the same as in the EPN case, with the only differences that windows have a potential different from that of the environment and that the deflector is at 0 (kV) Furthermore about 90 (kA) are needed to feed case 1 and 100 (kA) for case 2, to which the construction costs for the coils must be added. Finally is important to underline that the feasibility of this configuration depends strongly on the optimization of this coil.

Coils

The deflection of charged particles can also be produced by generating a uniform magnetic field, within which the ions, under ideal conditions, will move with uniform circular motion. In this section we will analyse the field produced by a toroidal coil and a square one, in order to identify the optimal configuration for our purpose.
Both coils that we will see now are single winding, since it is important to estimate the current necessary to generate the field and the fact that you can inject a smaller current, increasing the windings is only a technical aspect that is not relevant for yours purposes. For the same reason coils are made of air, in fact the difference in magnetic permeability of air and copper is negligible (air 1.2566375×10^{-6} (Hm^{-1}) , copper 1.2566290×10^{-6} (Hm^{-1})). Equations used by the mf module of COMSOL have already been defined in (section 3.2), for the operation of the simulation the program imposes the construction of an air domain (blue area) around the conductors, moreover, the program does not allow to simulate the field produced in the coils directly in the model of the recovery system, so it has been individually calibrated and subsequently exported to the MPN model.

4.5 Geometries

Circular turns are those that can generate the most uniform magnetic field, but they are more difficult from the point of view of maintenance. We analyse a toroidal coil and a square coil, that follows the vessel geometry, comparing the generated magnetic field, the thermal load on the collectors, the particle trajectories and the required supply current, in order to identify the best solution between the two and proceed with its optimization.
For the COMSOL analysis was used a free tetrahedral finer mesh.

4.5.1 Toroidal coil

The first solution is a toroidal coil with minor radius of 0.1 m, the major of 1.150 m. The coil is powered by current of 4.5×10^5 A injected along the inner circumference (Figure 4.35). In the first approximation it is centred with respect to the recovery system (Figure 4.36).

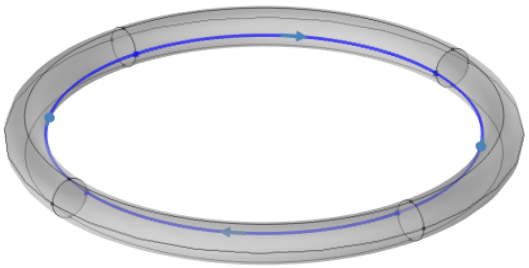

Figure 4.35: Toroidal coil input.

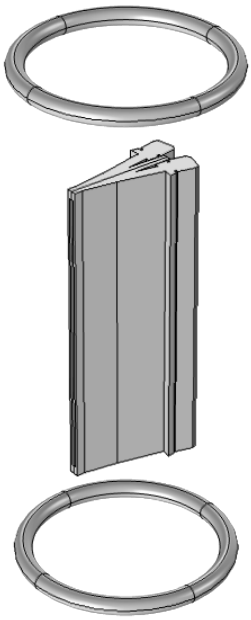

Figure 4.36: Recovery system and toroidal coil.

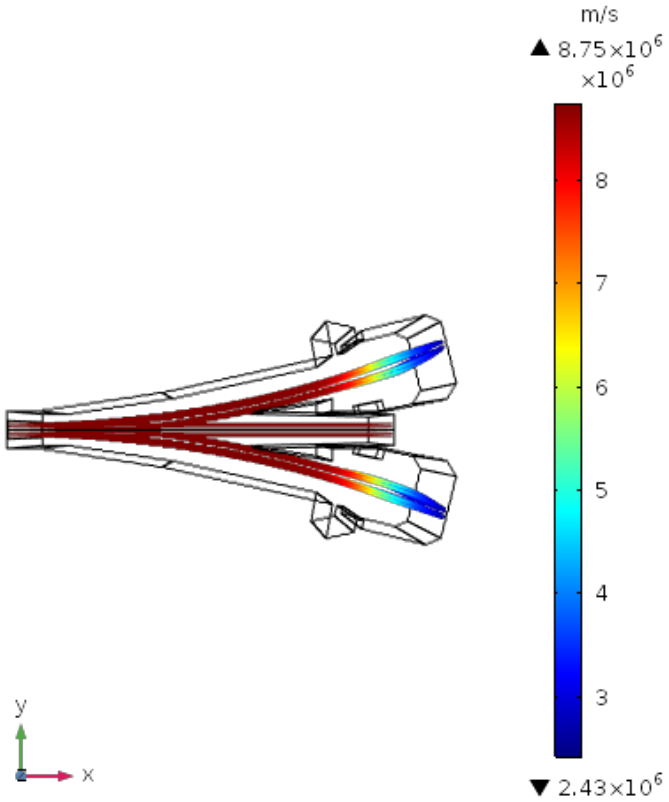

Figure 4.37: Trajectories of the particles for toroidal coil.

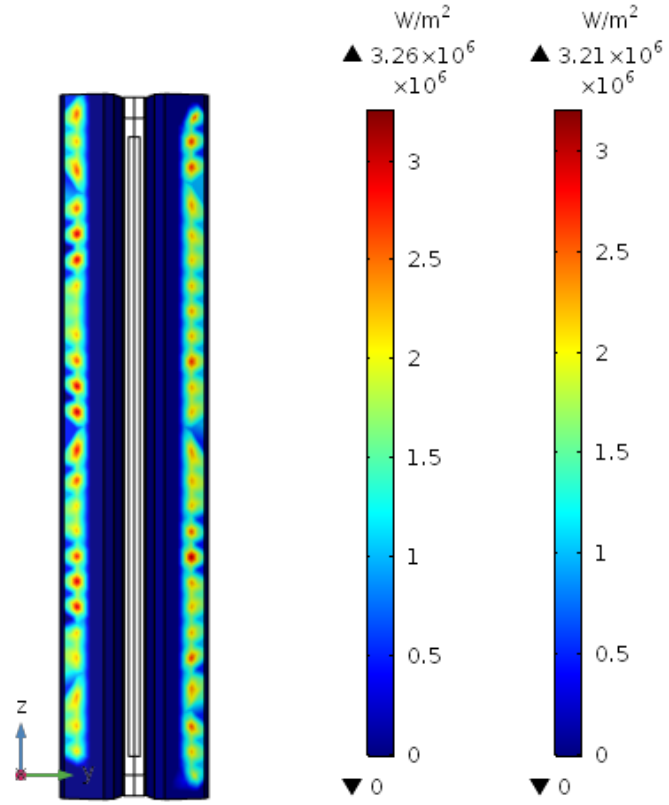

Figure 4.38: Thermal load for toroidal coil.

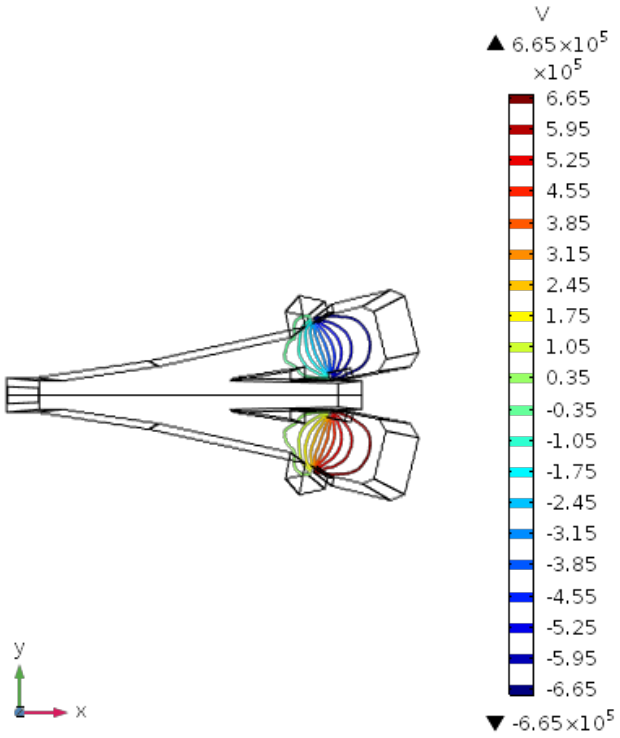

Figure 4.39: Lines of electrical potential for toroidal coil.

4.5.2 Square coil

The second one is a square coil that follows the shape of vessel. In reality the space available for the insertion of the coil is a rectangle, but being different from its sides by only 10 cm, it is better to opt for a square shape (2.3 (m) $\times$ 2.3 (m)) in order to obtain a better symmetry for the magnetic field, the current flowing there is of 5×10^5 (A) injected through a square section of the coil (Figure 4.40). Also in this geometry in first approximation it is centred with respect to the recovery system (Figure 4.41).

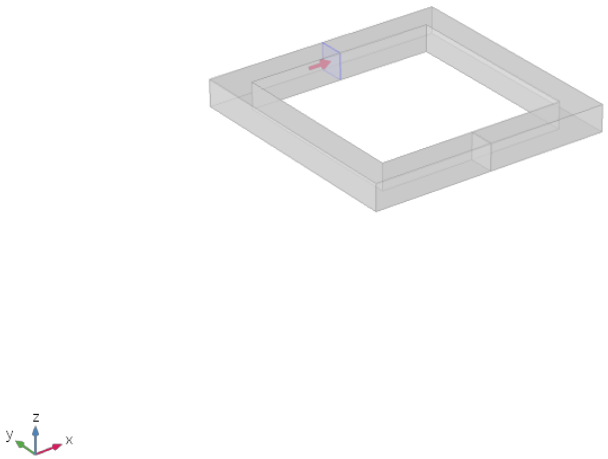

Figure 4.40: Square coil input for square coil.

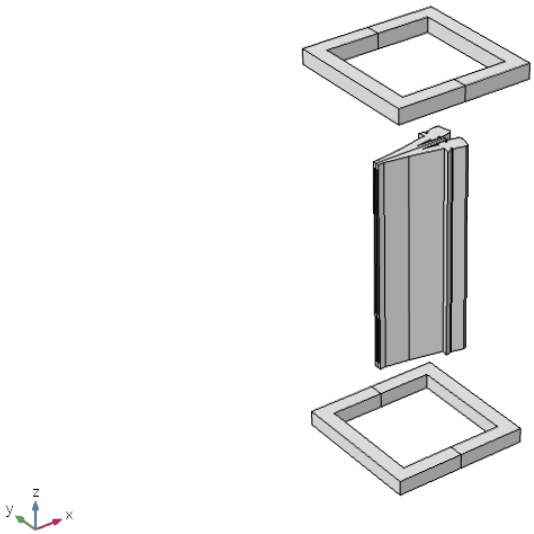

Figure 4.41: Recovery system and square coil.

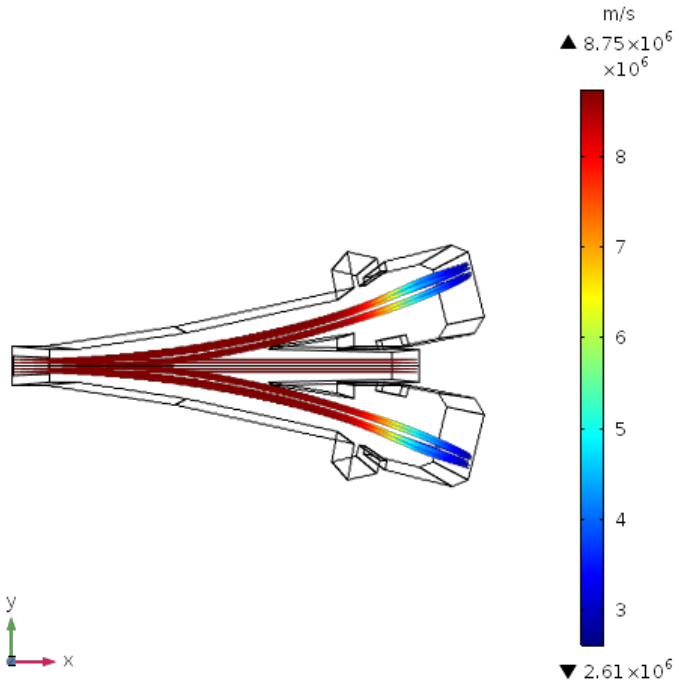

Figure 4.42: Trajectories for square coil.

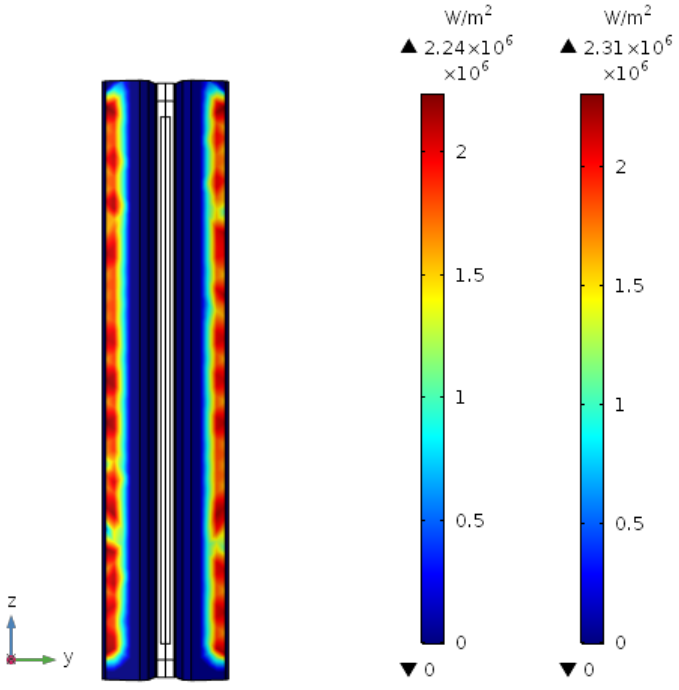

Figure 4.43: Thermal load for square coil.

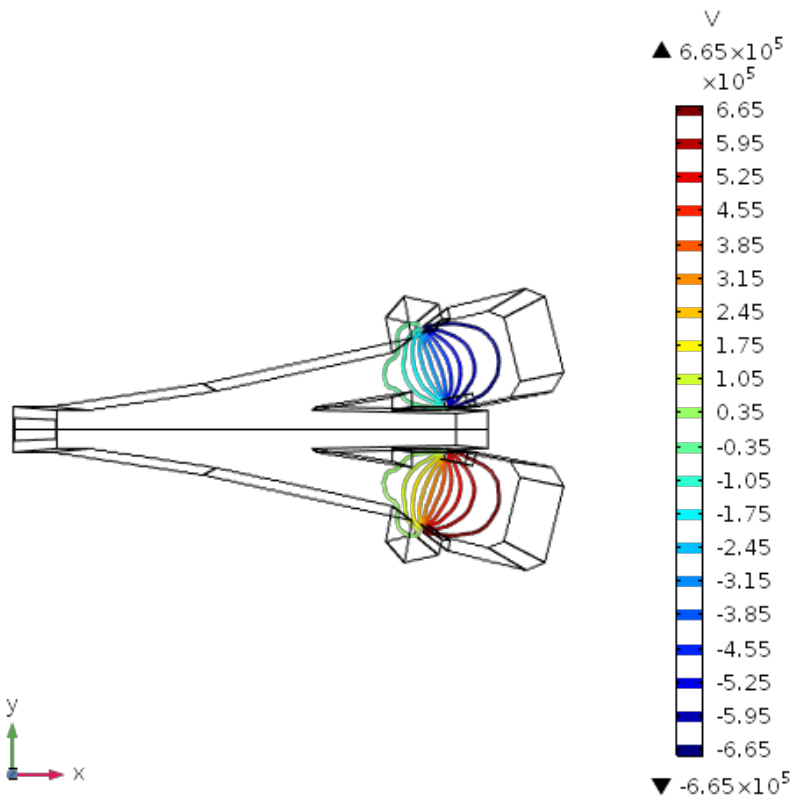

Figure 4.44: Lines of electrical potential for square coil.

4.5.3 Considerations

For all the solutions the use of a C in soft iron is also considered to optimize the field in the area of interest, but is not really useful, so it has not been included in the geometry to reduce size and costs. For the choice of the best form the following parameters were considered in order of importance:

1. Maximum heating power density;
2. Shape;
3. Current.

As for the thermal load, from figures 4.38 and 4.43 we can see that for the square coil this is slightly lower, moreover the shape of the latter is certainly easier to realize and facilitates maintenance interventions. The only advantage of the toroidal coil is that it requires a current of 50 (kA) lower than the square one, but due to the importance given to the parameters the square coil has been chosen as the best option.
An attempt has been made to reduce the dimensions, but a modification (even minimal) has considerable consequences on the uniformity of the magnetic field, with a consequent increase in the thermal load.
We report below a case of reduction of only 30 cm and the case of half-life:

External side (mm)	Internal side (mm)	Section side (mm)	Thermal load (W/m^2)	Current (A)
2300	1800	250	7×10^5	2.8×10^5
2000	1500	250	2.5×10^6	3.3×10^5
1150	900	125	2×10^6	8×10^5

It is evident that an intervention of this type only involves disadvantages, in fact the necessary current

increases by some tens of kA, and the thermal load increases by an order of magnitude. Shifts have also been made with the smaller coils, but no significant changes have been noticed, in fact the thermal load decreases compared to the non-shifted case, but the order of magnitude is still higher than in the case of maximum size. Figures 4.45, 4.46, 4.47 and 4.48 show the magnetic field of the square coil covered by a current of 50 kA:

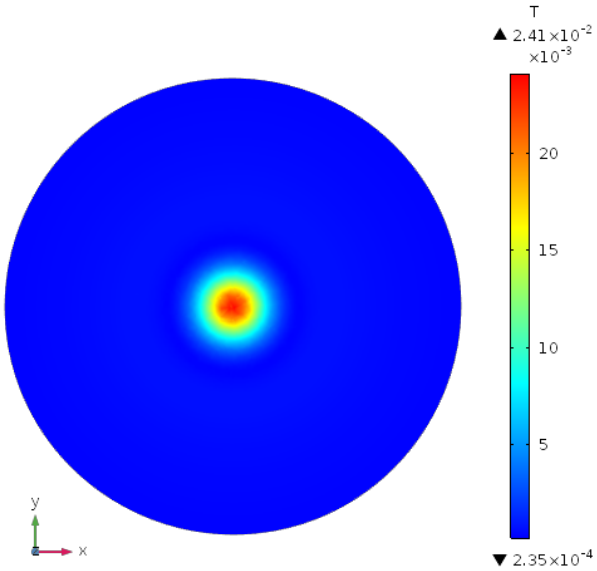

Figure 4.45: Magnetic flux density norm (T)

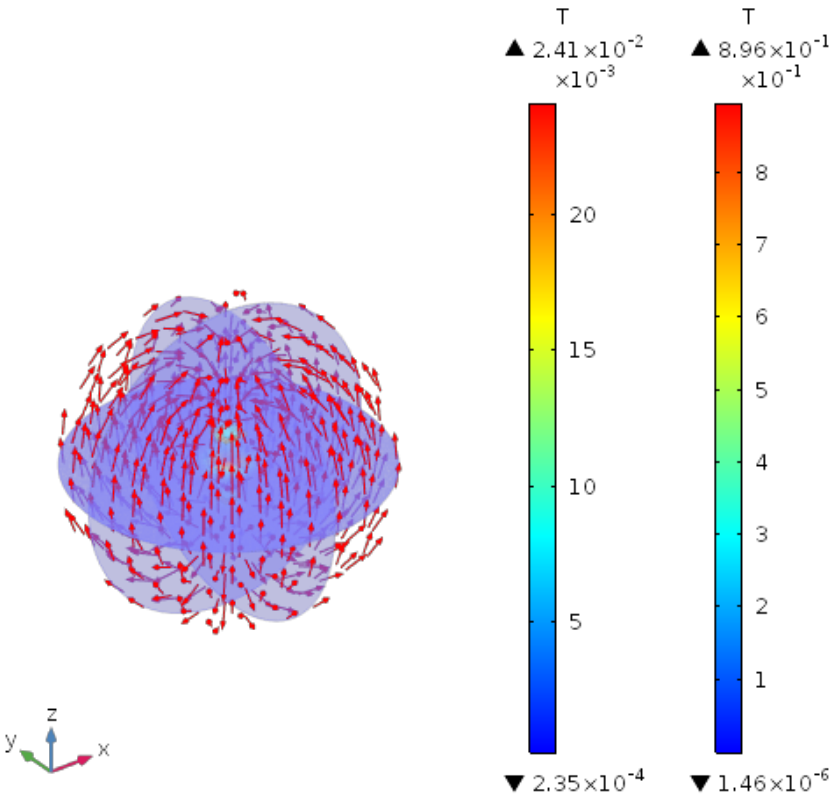

Figure 4.46: Magnetic flux density.

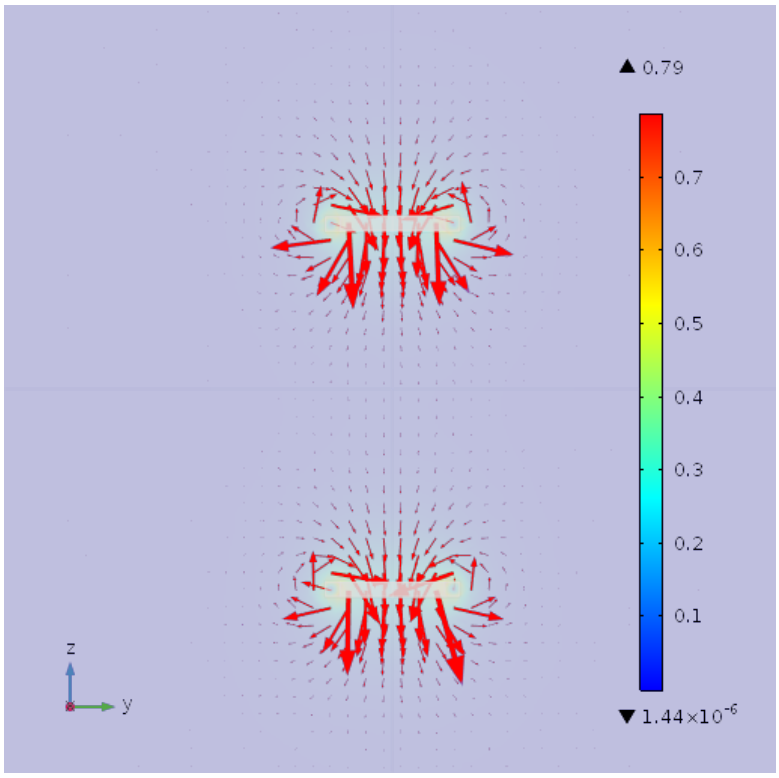

Figure 4.47: Magnetic flux density norm (T) and magnetic field (arrows)

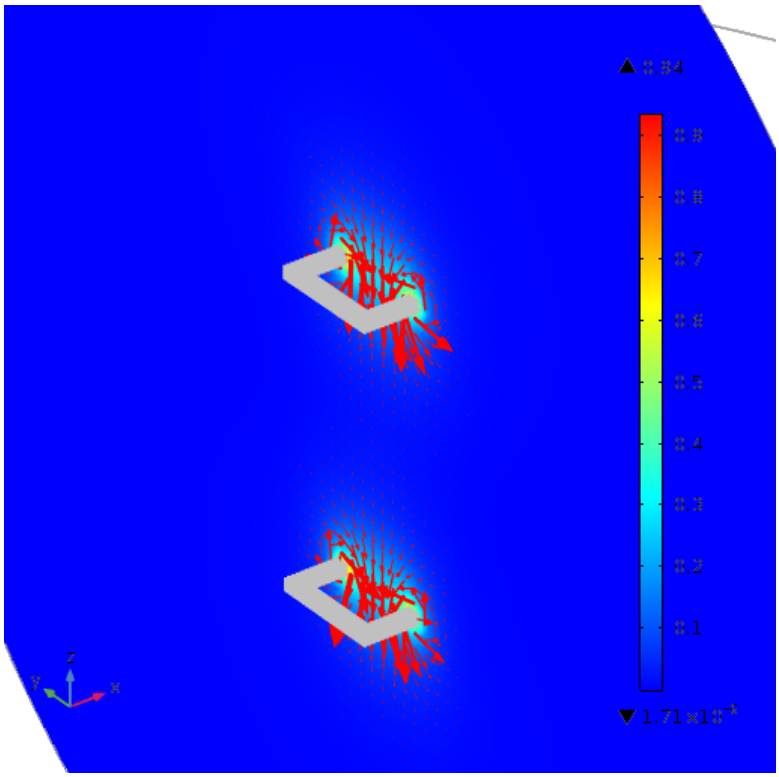

Figure 4.48: Magnetic flux density norm (T) and magnetic field (arrows)

Conclusion

Starting from the negative ion recovery system designed by J.Pamela and S.Laffite (chapter 2) two solutions have been proposed for DEMO (chapter 3.4) that, although having the same geometry, differ for the method used for the deflection of charged particles, in fact for EPN purely electric deflection was achieved through the use of potentials, while for MPN was generated a magnetic field through two square coils covered by current. For both configurations, an attempt was made to reduce the heat load on the manifolds first and then the amount of current required to supply a potential production in the future. For realization of MPN, a study was carried out on the coils (chapter 4) in order to identify the most performing one for the configuration. By carrying out simulations using COMSOL for the various configurations, the best current and potential values were identified, also verifying analytically (section 3.3) that the results obtained by FEM were consistent.
Before making a comparison, remember the cases discussed in the previous chapters:

Configuration	Deflection	Windows
EPN	Electric	Disabled (0 kV)
MPN(1)	Magnetic	Disabled
MPN(2)	Magnetic	Enabled (650 kV)

Let's now compare the two proposed ion recovery configurations choosing the best solution according to the principles of RAMI of DEMO. As seen that EPN configuration requires a voltage of about 1600 (kV) and the MPN one a current of about 90 (kA) plus a voltage of about 2700 (kV) (case 2) or a current of 100 (kA) plus a voltage of about 1400 (kV) (case 1) (we do not give precise values of these parameters, since this is a conceptual project that can certainly be optimized in the second phase).
Summarizing the results obtained we have:

Configuation	Max thermal load (Wm^{-2})	Current (kA)	Voltage (kV)	EI
EPN	5.15×10^6	/	1600	1
MPN(1)	2.31×10^6	100	1400	2
MPN(2)	1.16×10^6	90	2700	3

Where the values assigned to the implementation easiness (EI) are due to the fact that, in the case of EPN the fact that there are no coils makes the realization easier and cheaper, while between the two MPN the one with windows at the ambient potential is certainly easier to be implemented.
Thermal load remains the most important parameter (which is acceptable for values less than about $5{\times}10^6$ (Wm^{-2}) and you see that the results obtained are in favour of MPN(2), but you can see how EPN is easier to implement and less costly, and finally MPN(1) lies in between the two. It must also be considered that a single winding coil has been used for MPN, but in reality the current is inversely proportional to the number of turns, so the current can be reduced sharply.
For these reasons, the configuration with magnetic deflection and active windows (MPN(2)) appears to be the best among the alternating proposals.

Appendix

Below are all the acronyms used:

Acronym	Meaning
ITER	International Thermonuclear Experimental Reactor
DEMO	Demonstration Fusion Power Plant
RAMI	Reliability, Availability, Maintainability and Inspectability
NBI	Neutral Beam Injector
R&D	Research and Development
HVPS	High-Voltage Power Supplies
RID	Residual Ion Dump
NEG	Non-Evaporable Getter
FEM	Finite Element Method
EI	Easiness of Implementation

There are also three acronyms used in this thesis that indicate the three configurations treated for the ion recovery system:

1. Electrostatic deflection with negative ions recovery (EN);
2. Electrostatic deflection with positive and negative ions recovery (EPN);
3. Magnetic deflection with positive and negative ions recovery (MPN).

Bibliography

[1] https://www.iter.org/sci/iterandbeyond, (22/07/2018).

[2] P. Sonato, et al., *Conceptual design of the DEMO neutral beam injectors: main developments and R&D achievements*, Nuclear Fusion 57 (2017) 056026 (9pp).

[3] P. Sonato, et al., *Conceptual design of the beam source for the demo Neutral Beam Injectors*, New J.Phys 18 (2016) 125002.

[4] P. Agostinetti and P. Sonato, *Optics and Thermo-Mechanical Analysis of the Accelerator for the DEMO Neutral Beam Injector*, Submitted to IEEE transaction on plasma science.

[5]J. Paméla and S. Leffite,*Conceptual study of a purely electrostatic energy recovery system for negative-ion-based neutral beam injectors*, Nuclear Instruments and Methods in Physics Research A295 (1990) 453-460 North-Holland.

[6] J. Paméla, et.al, *Measurement of the neutral and charged beam fractions in a D^- 100 keV 2 A neutral beam injector* Nuclear Instruments and Methods in Physics Research B73 (1993) 289-295 North-Holland.

[7]J. Paméla, et al., *Energy recovery experiments with a a powerful 100 keV D^- based neutral beam injector* Nuclear Instruments and Methods in Physics Research B73 (1993) 296-302 North-Holland.